EMU Notes in Mineralogy, Vol. 11 (2011), Chapter 4, 151–202

Modelling of X-ray diffraction profiles: Investigation of defective lamellar structure crystal chemistry

BRUNO LANSON

Mineralogy & Environments, Institut des Sciences de la Terre, Université Joseph Fourier – CNRS, 38041 Grenoble cedex 9, France
e-mail: bruno.lanson@obs.ujf-grenoble.fr

Layered minerals and materials are ubiquitous and characterized by the frequent occurrence of stacking defects. In particular, interstratification (or mixed layering), which corresponds to the intimate intergrowth of layers differing in terms of their layer thickness and/or internal structure, and stacking faults, both random and well defined, are especially common. These defects impact heavily on the reactivity of the lamellar structures. In addition, they may record the conditions of mineral (trans)formation. Determining their nature, abundance and possibly their distribution is thus an essential step in their structural characterization leading to an understanding of their reactivity. Over recent decades, modelling of X-ray diffraction profiles has proved to be an important tool which allows detailed structural identification of defective lamellar structures. The present chapter will review the basic concepts of such identification and review the literature to outline how our understanding of defective structures and mixed layers has improved over the last decade or so and to describe some of the new perspectives opened by this improvement.

1. Introduction

Layered compounds are ubiquitous on Earth as minerals (*e.g.* clay minerals and layered oxides) but also as geogenic or synthetic materials (*e.g.* carbons, layered double hydroxides, layered dichalcogenides, high-temperature superconductors). In contrast to pseudo-layered compounds, they are characterized by interatomic bonds much stronger within two-dimensional fragments/layers than between these fragments. The sustained interest in these structures arises from their reactivity which is reinforced by

This chapter is dedicated to some of those who have initiated, guided, encouraged or helped the development of my scientific activity through the years. The long-term interaction with Victor A. Drits has been an essential and inexhaustible source of inspiration, knowledge and motivation. Curiosity and stimulation also resulted from reading Robert C. Reynolds' writings and listening to his talks. Alain Meunier and Bruce Velde guided my first steps into the magical world of clay science. Alain Manceau made possible to develop my academic activity and brought both scientific rigour and opportunities to it. Gérard Besson, Alain Plançon and Boris A. Sakharov shared their experience and knowledge of diffraction effects arising from defective structures. Finally, PhD students, especially Anne-Claire Gaillot, Francis Claret, Eric Ferrage and Sylvain Grangeon, carried out a significant part of the daily simulation work and brought innovative ideas to it. To all, thank you very much both for your scientific input to this work but also for the associated human dimension. To Martine, Bertrand, Meije and Robin, thank you for your love, patience and understanding.

DOI: 10.1180/EMU-notes.11.4

their anisotropic character. In particular, the intercalation properties of lamellar compounds have drawn the attention of the materials chemistry community for several decades in an effort to prepare polyfunctional materials. Similarly, the reactivity of natural layered silicates in response to their environmental conditions has been investigated thoroughly both for its potential ability to record temperature and/or pressure palaeo-conditions, and to assess the possible impact of these minerals on their environment, in particular in the context of waste storage.

Layered materials and minerals commonly exhibit a high density of structure defects. These defects range from local defects such as isomorphous substitutions, layer vacancies, or atomic displacements, to random or well defined stacking faults induced by non-periodic layer rotations, translations or twinning, and to interstratification (or mixed layering, both terms being used hereafter as synonymous) resulting from the coexistence within a given crystal of layers having different structure, thickness, or interlayer displacement. The occurrence of stacking faults in lamellar structures is favoured by the energetic similarity of the different stacking modes, owing to the weak interactions between adjacent layers. In addition, layered materials and minerals often exhibit minute crystal sizes that may be considered as an additional type of defect because of the induced disruption of the three-dimensional (3D) crystal periodicity.

The reactivity of lamellar structures actually depends, to a large extent, on these structure defects, on their nature, abundance and distribution within crystals. This influence is exemplified by the direct relationship between surface area and reactivity, or by the specific amphiphilic properties of layered silicates when intercalated with hydrophilic and hydrophobic species in successive interlayers (*e.g.* Ijdo & Pinnavaia, 1998a, 1998b). These structure defects also exert an essential influence on the actual physicochemical properties of these layered structures. Similarly, structure defects are often considered as indicators of the mineral conditions of formation. It is therefore essential to determine these parameters to gain additional insight into these physicochemical conditions in an effort to reconstruct reaction pathways, and/or to predict the reactivity of a given material/mineral. To establish these interpretations on scientifically sound bases, a detailed structural characterization of defective lamellar structures is thus essential, and X-ray diffraction (XRD) has been the preferred method of investigation.

However, as a result of their non-periodicity or their reduced periodicity, the diffraction maxima recorded from these compounds do not strictly obey Bragg's law, thus hampering the use of conventional diffraction approaches, such as the Rietveld method. Profiles and intensities of diffraction maxima are affected by the nature, abundance, and distribution of structure defects, however, thus allowing the determination of these parameters with diffraction techniques. Drits (1997, 2003) stressed the remarkable ability of diffraction techniques to extract average structural information from crystals deprived of 3D periodicity. This author also pointed out that the reliable determination of structural and chemical heterogeneity of layered structures depends essentially on the reliable interpretation of diffraction data.

In this chapter some of the literature from the last two decades is reviewed to: (1) provide a description of the different types of structure defects that may be encountered in layered structures and of their influence on XRD patterns; (2) provide insights into the

XRD data processing specific to these defective structures and into the structural information that can be retrieved; and (3) provide a review of the recent literature describing the nature, abundance and distribution of structure defects in layered silicates, layered oxides and layered double hydroxides.

2. General background on structure defects and induced diffraction effects

2.1. Different structure defects

2.1.1. Local defects

Layered structures commonly possess complex chemical compositions together with a wide spectrum of isomorphic substitutions of cations or anions, including the presence of vacant sites. It should be noted that local defects essentially affect the structure factor by modifying the average unit-cell content. As a consequence, this type of defect can be described by the usual structural methods allowing the calculation of diffracted intensity by a given structure, such as the Rietveld refinement, and will not be detailed here. An important side effect of the high density of local defects is the minute crystal size of these lamellar minerals and materials (Meunier, 2006). This finely divided character has essential implications both for the reactivity of these structures and for their XRD signature, inducing in particular a significant peak broadening that increases as a function of $1/\cos\theta$ (Scherrer, 1918; Guinier, 1964).

2.1.2. Stacking defects

In layered structures, the weak interactions between adjacent layers result in the energetic similarity of different stacking modes, and thus to the frequent occurrence of stacking faults. In particular, stacking faults may be due to random rotation and/or translation between consecutive layers. When the extent of the random translation is limited and does not totally disrupt the scattering coherence of adjacent layers, faults may be described as fluctuations of the translation vectors about a mean value. Depending on the nature of the interactions between the layers and on the physical reasons for the translations' variations, such fluctuations were shown to be of two types (Guinier, 1964; Drits & Tchoubar, 1990). In the first type (Fig. 1), fluctuations follow a unique law for any layer pair, and this law thus describes both short- and long-range order in a layer stack. As a result, the total translation between two nth-nearest neighbour layers is equal to n times the average translation, although the translation may vary from one layer pair to the other. The effect of this type of defect is similar to the thermal motion of atoms and is characterized by a loss of intensity when increasing the diffusion vector (**s**), which is directly related to the diffraction angle ($s = (2 \times \sin\theta)/\lambda$). In the second type of fluctuations, there is no long-range correlation between the defects and the total translation between two nth-nearest neighbour layers is then no longer equal to n times the average translation. The influence of this type of defect on the XRD patterns is stronger than that of the first type, leading both to a significant intensity decrease and to peak broadening when increasing the diffusion vector.

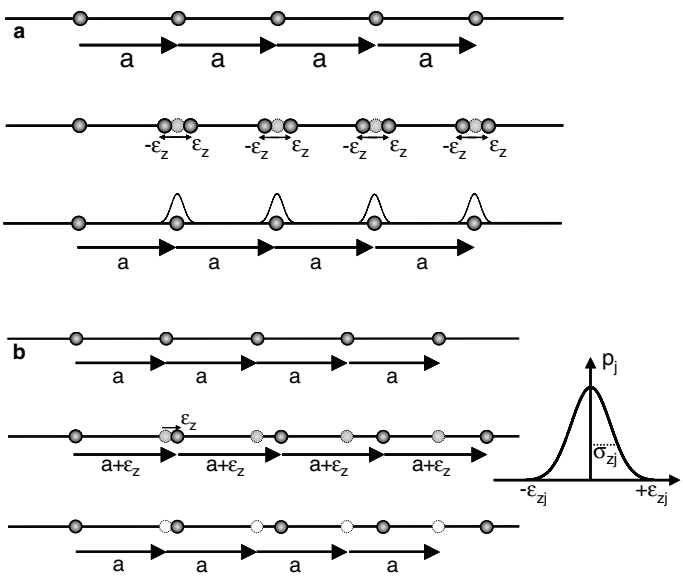

Fig. 1. Schematic description of translation vector fluctuations. (***a)*** Fluctuations of the first type. (***b***) Fluctuations of the second type (see text for details – adapted from Ferrage, 2004). **a** represents the translation vector and ε_z the additional displacement that occurs with a p_j probability.

In contrast to fluctuations of the translation vectors, random stacking faults are characterized by a translation between adjacent layers the direction and amplitude of which are random, thus leading to a strikingly different distribution of deviation from the average translation (Drits & Tchoubar, 1990). When they occur, such random translations statistically disrupt the interferential coherence of the substacks between which they occur. As a result, these substacks behave independently from each other from a diffraction point of view, and the resolution of *hkl* reflections is progressively lost when increasing the proportion of such random stacking faults (Fig. 2). Random rotations induce the same effect. When random stacking faults occur systematically between successive layers (turbostratic stacking), unresolved *hkl* reflections lead to an asymmetric profile called *hk* diffraction band, characteristic of two-dimensional crystals, similar to that obtained from a single layer. These diffractions bands display a rapid increase of the diffracted intensity near the value $s_0 = |h\vec{a}^* + k\vec{b}^*|$ followed by a slow decrease.

Finally, well defined stacking faults may occur between successive layers with a given probability. In this case, it is possible to consider that different layers, characterized by their own unit-cell parameters and structure factors, coexist within the same crystals, and the diffraction effects are similar to those arising from mixed layers and described in the next section.

2.1.3. Interstratification

Mixed layers are remarkable examples of order-disorder observed in natural and synthetic lamellar crystals. They consist of the alternation either of layers exhibiting

contrasting structures, compositions and basal distances or of layers having similar basal distances but differing by their internal structures or stacking mode, that is exhibiting different layer displacement or rotation between consecutive layers. The different layer types can coexist in variable proportions within the crystal and define a variety of layer stacking sequences. Mixed layering (or interstratification) has been widely recognized in natural and synthetic species such as layered silicates, layered manganates, hydrotalcites and synthetic layered double hydroxides, layered oxides in general, sulphides and intercalated graphites.

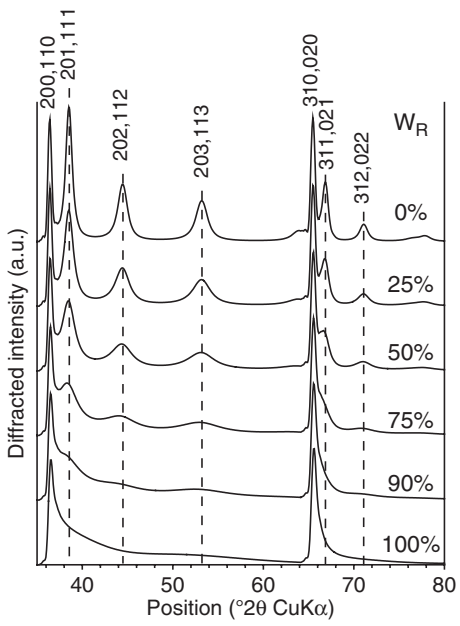

Fig. 2. Influence of random stacking faults on XRD patterns calculated for a layered manganese oxide (1*H* birnessite – adapted from Grangeon, 2008). W_R represents the occurrence probability of random stacking faults.

Two main categories of mixed layers can be established, depending on the actual distribution of interstratified layer types. The first type of mixed layers corresponds to regular structures in which different layer types alternate periodically, usually along the axis perpendicular to the layer plane (c^* axis). These mixed layers have, in many cases, been given mineral names, as they have strictly periodic structures and are often considered as distinct phases. Chlorites and corrensite are two examples of such structures that can be described as regular talc-brucite and chlorite-smectite, respectively. Within the materials-chemistry community these regular alternations of different layer types are known as the 'staging' phenomenon, the *n*th staging corresponding to the systematic occurrence of a given layer type at every *n*th layer (Fogg *et al.*, 1998a; Ijdo & Pinnavaia, 1998b). When the different layer types have the same structure but differ from their layer displacement, their regular alternation defines polytypic variants of a given mineral/species.

In the second type of mixed layers, the different layer types either alternate at random or tend to some sort of ordering (avoiding for example the existence of pairs of the minor layer type) or segregation (clustering layers of a given type). In this case and if interstratified layers have significantly different thicknesses and structures (Fig. 3), resulting peak positions do not obey Bragg's law but form a non-rational series ($d_{001} \neq l \times d_{00l}$) leading to the apparent lack of physical meaning for the observed peak positions. For a given composition, *i.e.* for given relative proportions of the different layer types, the actual position of the diffraction maxima corresponding to such a mixed layer depend on the actual layer sequences and on their relative abundances (see section 2.2.2.).

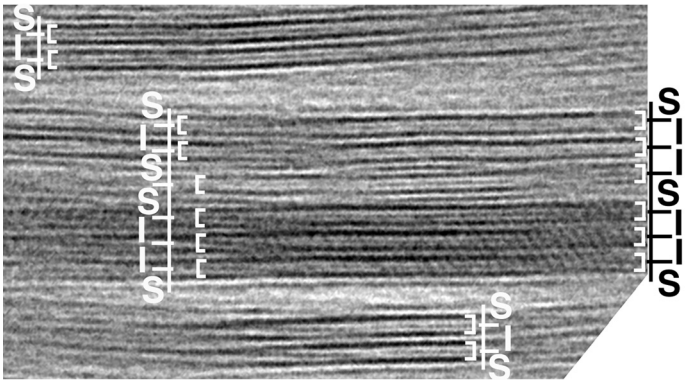

Fig. 3. Transmission election microscope (TEM) image of an illite-smectite sample (adapted from Murakami *et al.*, 2005). Brackets outline the T-O-T silicate layers; I and S accompanied by a pair of bars indicate illitic and smectitic layers, respectively. Bars near I or S are located at the centre of an octahedral cation plane. The distance between a pair of bars with I is 1.0 nm.

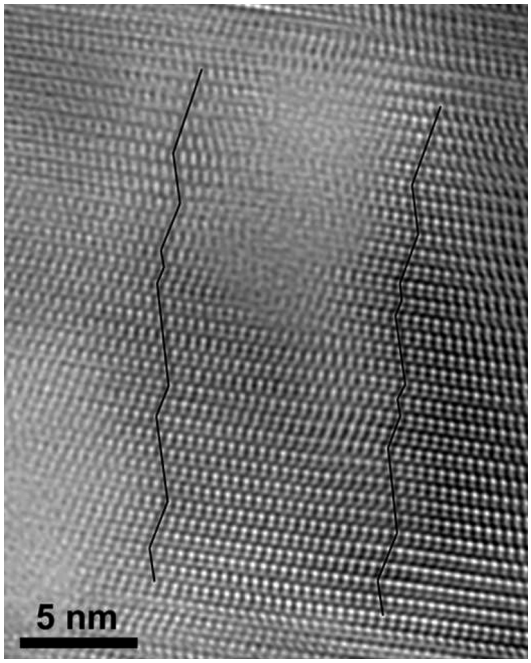

Fig. 4. Filtered high-resolution TEM image of a kaolinite crystal along one of the x_i directions (adapted from Kogure *et al.*, 2010). The solid lines connect equivalent points in successive layers and the direction changes correspond to the occurrence of well defined stacking faults.

The second type of mixed layers also includes structures in which the respective thicknesses of interstratified layers are multiples of each other (*e.g.* chlorite-serpentine). In this case, the positions of reflections corresponding to the mixed layer form a rational series, and the determination of the interstratified character of the structure then requires a more detailed analysis of peak position, profiles (especially width) and relative intensities for different reflections (Moore & Reynolds, 1997; Drits, 2003).

Finally, the second type of mixed layers includes structures in which interstratified layers have about the same thickness but distinct structures or layer displacement (Fig. 4). In this case, only the positions of non-basal reflections are affected. These reflections form non-rational series as basal reflections for mixed layers in which interstratified layers have significantly different

thicknesses and structures. Within this last type of mixed layers, additional variety can arise from the possible incommensurability of the interstratified layers within the *ab* plane.

Although occurrences of interstratification reported in the literature correspond overwhelmingly to the coexistence of two layer types, both the occurrence and the description of mixed layers containing three, or more, layer types are possible. Over the last decade or so, the quantitative assessment of diffraction data has proven that such complex mixed layers may actually be extremely common; the main reasons for their rare description in the literature being: (1) the absence of a direct quantitative comparison between experimental and calculated patterns; and (2) the non-availability of adapted calculation routines.

2.2. Interpretation of diffraction data from disordered solids

Drits (2003) stressed the possibility of extracting average structural information from the diffraction patterns obtained on crystals lacking 3D periodicity. However, interpretation of XRD effects from defective compounds cannot be achieved satisfactorily with conventional XRD methods such as single-crystal diffraction and/or Rietveld structure refinement using powder diffraction data because of this reduced periodicity. This has led to the development of specific algorithms for the calculation of diffraction effects arising from defective structures.

2.2.1. Crystals exhibiting local defects and/or random stacking faults

The common occurrence of isomorphic cation or anion substitutions, including the presence of vacant sites, in layered structures essentially modifies the calculation of the structure factor. It is thus not specific to defective compounds and is accounted for by usual structural methods allowing the calculation of the intensity diffracted by a given structure. Although not described specifically in the present chapter, local defects should, however, be included in a comprehensive structural characterization of defective compounds.

Warren (1941) was among the first to propose a formalism that describes the diffraction effects arising from the presence of random stacking faults in lamellar crystals (Drits & Tchoubar, 1990; Leoni, 2008). This formalism allows us to extract structural information from the profile of *hk* bands, despite the absence of resolved *hkl* lines (Biscoe & Warren, 1942; Manceau *et al.*, 2000a; Villalobos *et al.*, 2006).

Recently, alternative approaches have been proposed to retrieve structural information from XRD patterns of such two-dimensional (2D) compounds. The first is based on the recursive description of the stacking of layers (Treacy *et al.*, 1991; Leoni *et al.*, 2004; Tsybulya *et al.*, 2004; Leoni, 2008); the second is based on the Rietveld algorithm (Rietveld, 1967; Ufer *et al.*, 2004). Both approaches have in common the ability to minimize 'automatically' the difference between experimental and calculated patterns. However, both rely on 'tricks' to mimic the diffraction behaviour of 2D periodic compounds. In the first case, as the stacking vector between successive layers must be defined, turbostratism is described as the random succession of different well defined

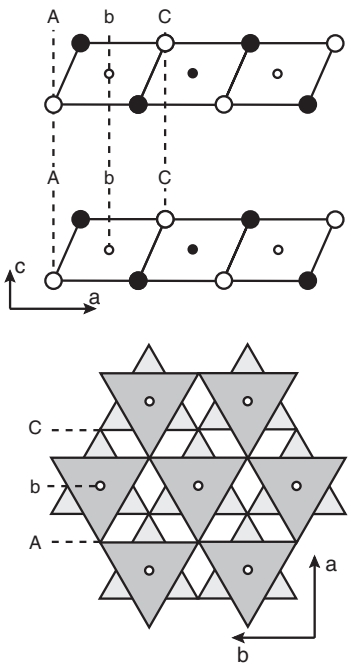

Fig. 5. Idealized structure model of layer stacking in a 1*H* polytype, or *hcp* (adapted from Drits *et al.*, 2007a). Top: projection along the **b** axis. Open and solid symbols indicate atoms at $y = 0$ and $y = \pm\frac{1}{2}$, respectively. Large circles represent O_{layer} atoms and small circles represent Mn_{layer} atoms in the phyllomanganate birnessite. Dashed lines outline specific positions of the close-packing formalism. Bottom: projection on the *ab* plane. The upper surface of the lower layer is shown as light-shaded triangles whereas the lower surface of the upper layer is shown as dark-shaded triangles. Mn_{layer} of the upper layer are shown as small open circles.

vectors (Leoni *et al.*, 2004). In the second case, the calculation of *hk* bands is performed for a large super-cell along the axis perpendicular to the layer plane, this super-cell containing a single layer. The resulting calculation is about equivalent to that performed for an equivalent super-cell containing several layers randomly shifted (Ufer *et al.*, 2004). However, in the latter case, several calculations need to be performed and averaged to smooth out the *hkl* oscillations. The two types of calculations lead to XRD patterns similar to those obtained assuming random stacking faults (Ufer *et al.*, 2004). Recently, recursive description of layer stacking has also been implemented in the *BGMN* code which aims to improve the description of turbostratic structures (Ufer *et al.*, 2008).

2.2.2. Well defined stacking defects/interstratification

In addition to the above-described random stacking faults, lamellar compounds are characterized by the frequent occurrence of stacking faults corresponding to a well defined translation and/or rotation between adjacent layers. For example, using the close-packing notation, 1*H* layer stacking of an octahedral sheet may be described as AbC AbC AbC ... (Fig. 5). The presence of well defined faults can alter the periodicity of such stacking leading, for example, to an AbC AbC CbA CbA ... sequence (twinning – Fig. 6), or to an AbC AbC BcA BcA ... one ($+a/3$ layer displacement). Similarly $3R^-$ polytypes can be described as AbC CaB BcA AbC ... using the same close-packing notation. In this case, the occurrence of a '1H' fault corresponds to a null, rather than $-a/3$, layer displacement between two consecutive layers and results in an AbC AbC CaB BcA AbC ... sequence (Fig. 7). Such stacking faults can be described as the interstratification of different polytypic fragments.

From the diffraction point of view, the description of non-periodic crystals resulting from the presence of well defined stacking faults requires the definition of the fault nature, *i.e.* of the corresponding translation vector, of its abundance and of the probability law for its occurrence. The exact same set of parameters is required to describe the interstratification of layers having similar unit-cell parameters within the layer plane

but different layer-to-layer distance. The intrinsic non-periodicity of crystals exhibiting such stacking faults, which include interstratification, hampers their structural characterization with conventional XRD methods such as single-crystal diffraction and/or Rietveld structure refinement using powder diffraction data. This has led to the development of specific algorithms for the calculation of diffraction effects arising from such defective structures consisting of layers having identical or different thicknesses.

MacEwan (1956) and D'yakonov (1961, 1962) proposed direct methods for the structural analysis of mixed layers. These methods, especially that implemented by D'yakonov (1961, 1962), have been used, especially in the former USSR, to determine the thickness and relative proportions of the different layer types coexisting in mixed layers (Drits & Tchoubar, 1990 and references therein). They present several intrinsic limitations that prevent general use, however. In particular, Drits & Tchoubar (1990) outlined the inadequacy of this method to deal with mixed layers whose stacking sequences depart significantly from the maximum possible degree of ordering (MPDO) case (see section 2.3.1.). In addition and more importantly, these methods are inefficient when different phases coexist in a sample leading to overlapping reflections.

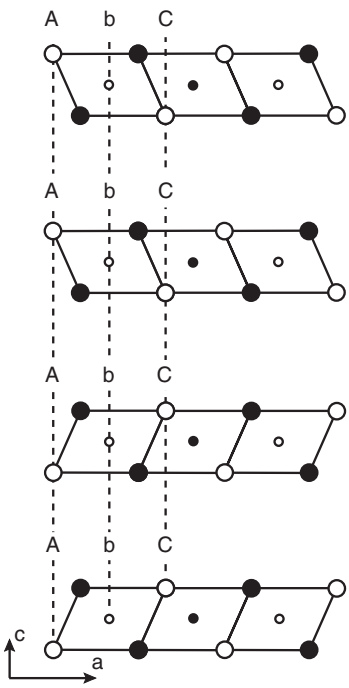

Fig. 6. Idealized structure model describing the occurrence of a twinning fault in a 1*H* polytype. The resulting sequence is described as AbC AbC CbA CbA ... using the close-packing formalism. Symbols as in Figure 5.

Alternatively, and at about the same time, indirect methods have been proposed that allow the calculation of diffraction effects arising from non-periodic interstratified structures. Hendricks & Teller (1942) were the first to propose an elegant matrix formalism allowing the calculation of diffraction effects arising from an infinite stack of interstratified layers. This formalism was further improved over the years, in particular to account for the limited extension of crystals and for a wider variety of stacking sequences (Méring, 1949; Kakinoki & Komura, 1952, 1954a, 1954b, 1965; Allegra, 1961, 1964; Cesari *et al.*, 1965; Cesari & Allegra, 1967). This formalism is still widely used, in particular among the clay community, to describe the intensities of basal (00*l*) and *hkl* reflections diffracted by a set of crystals containing different layer types (Drits & Sakharov, 1976; Plançon, 1981, 2002; Sakharov *et al.*, 1982a, 1982b; Watanabe, 1988; Drits & Tchoubar, 1990).

Another approach, which is based on the direct summation of the contributions to diffracted intensity coming from waves scattered by all possible layer subsequences in the interstratified crystals, was also developed for the calculation of XRD patterns from mixed layers (Reynolds, 1967, 1980). Finally, Treacy *et al.* (1991) proposed a recursive

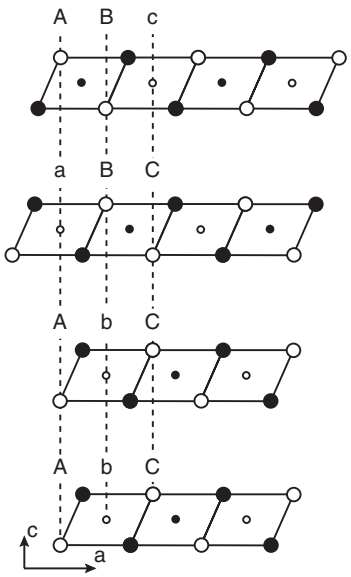

Fig. 7. Idealized structure model describing the occurrence of a 1*H* fault in a $3R^{-}$ polytype. This fault corresponds to a null, rather than $-a/3$, layer displacement between two consecutive layers and results in an AbC AbC CaB BcA AbC ... sequence. Symbols as in Figure 5.

method for describing layer stacking in lamellar compounds exhibiting well defined stacking faults and/or interstratification and for calculating diffracted intensities from such compounds. This program was implemented in the *DIFFaX* code (Treacy *et al.*, 1991; Leoni *et al.*, 2004), which is used widely by the 'materials community'.

The determination of a structure model using one of these approaches usually relies on the comparison of XRD profiles calculated for a structure model with the data. The optimum fit to the data, and thus the selection of a structure model, is commonly obtained by a trial-and-error procedure. Attempts have been made to couple the above-described approaches with minimization routines in an effort to reduce the time needed to reach an optimum solution. Benefiting from the sustained interest of the oil industry for the potential of mixed layer as indicators of temperature palaeo-conditions, genetic algorithms were, for example, coupled to the Reynolds method (Pevear & Schuette, 1993) or more recently to the matrix formalism (Aplin *et al.*, 2006). Similarly, non-linear least-squares minimization routines have been coupled both to the *DIFFaX* code (Leoni *et al.*, 2004) and to the matrix approach (Plançon & Roux, 2010). The recursive approach has also been included in the general-purpose Rietveld code *BGMN* (Bergmann & Kleeberg, 1998; Ufer *et al.*, 2004, 2010). These efforts towards the coupling of routines allowing the calculation of diffraction effects from defective structures with minimization routines are beneficial, and probably necessary, for the development of these methods and of a more systematic quantitative assessment of the structure models proposed for such defective structures. Care must be taken, however, to avoid reducing the flexibility of the calculation routines while implementing the coupling.

2.3. XRD identification of defective structures

2.3.1. Calculation of XRD intensity from mixed layers

The calculation of diffraction effects arising from mixed layers would need a separate chapter of its own to enable a thorough description. It is beyond the scope of the present chapter. The interested reader will find relevant information on the direct summation method, on the recursive approach, and on the matrix formalism in Reynolds (1980, 1989) and Moore & Reynolds (1997), in Treacy *et al.* (1991) and Leoni *et al.* (2004), and in Drits & Tchoubar (1990), respectively.

Using the simple and elegant matrix formalism, the expression of the intensity diffracted by mixed layers has remained unchanged since the early works of Kakinoki & Komura (1952, 1954a, 1954b) and may be expressed as:

$$I = NSpur[V][W] + 2\mathrm{Re}\sum_{n=1}^{N-1}(N-n)Spur[V][W][Q]^n \qquad (1)$$

where $[V]$ is the square matrix containing the structure factors, $[W]$ the diagonal matrix containing the occurrence probability of the different layers, layer pairs, layer triplets, ... depending on the extent of the ordering parameter (S or Reichweite – Jagodzinski, 1949), and Q a square matrix of the product of junction probabilities describing layer stacking sequences by the corresponding phase term. S*pur* is the trace of a matrix, that is the sum of its diagonal elements, and N is the number of layers in a given crystal (Drits Tchoubar, 1990). The contents of the matrices $[V]$, $[W]$ and $[Q]$ depend on the structural model characterized by a given number of layer types and a short-range order factor, S (Reichweite, often reported in the literature as the R parameter).

To calculate diffraction effects arising from a mixed layer, the first requirement is thus to determine the number of the different layer types and their respective structures. Unit-cell parameters, together with atomic coordinates and occupancies of the different layer sites, are indeed necessary to define the structure factors and phase terms. For lamellar compounds exhibiting well defined stacking faults, the requirements are essentially the same, except that the different layer types are distinguished from their different stacking vectors within the *ab* plane. The next requirement is to describe the stacking sequences of the different layer types. For this, different sets of probability parameters are required. At first, it is necessary to determine the relative proportions (W_i) of the different layer types. Next, an essential parameter to be defined is the short-range order factor, S (Reichweite). This Reichweite parameter was originally proposed by Jagodzinski (1949) to describe how many of its neighbours will influence the presence of a given layer. Following this definition, the Reichweite parameter, S, can only have integer values. On the other hand, if this parameter defines the extent of the influence of a given layer, it provides no indication as to the nature of this influence, which is characterized by junction probability parameters. These probability parameters define the probability of finding a layer type (j) after a given layer type (i) and are usually denoted P_{ij}.

Although different models may be used to define these parameters (Plançon *et al.*, 1983, 1984a, 1984b), the quasi-homogeneous model that assumes Markovian statistics is overwhelmingly used in the literature (Kakinoki & Komura, 1952, 1954a, 1954b, 1965; Drits & Sakharov, 1976; Reynolds, 1980; Drits & Tchoubar, 1990). For illustration purposes, one may consider the case of mixed layers containing two layer types (A and B) and different sets of junction probability parameters. If one first assumes that S, the Reichweite parameter, is equal to 1 only four junction probability parameters (P_{AA}, P_{AB}, P_{BA} and P_{BB}) are required, together with the relative layer abundances (W_A and W_B) to thoroughly describe layer-stacking sequences.

These six parameters are linked by the following four relations:

$$W_A + W_B = 1 \quad (2)$$

$$P_{AA} + P_{AB} = 1, \text{ and } P_{BA} + P_{BB} = 1 \quad (3)$$

$$W_A \times P_{AB} = W_B \times P_{BA} \quad (4)$$

The rationale for equation 2 is obvious. The two parts of equation 3 state that a given layer (A or B) can be followed only by A or B layers. From the first part of equation 3, it is clear that $W_A = W_A \times P_{AA} + W_A \times P_{AB}$. Similarly, the occurrence probability of A layers can be written as $W_A = W_A \times P_{AA} + W_B \times P_{BA}$, and equation 4 can easily be derived from the combination of the last two equations. As a result, there are only two independent parameters among the six probability parameters needed to describe stacking sequences in a two-component mixed layer with $S = 1$. One of these parameters should be W_A, or W_B. If $W_A > W_B$, it is convenient to choose P_{BA} or P_{BB} as the second independent parameter as their values may vary from 0 to 1. If, for example, P_{BB} is the independent parameter, then other probabilities can be defined as:

$$W_B = 1 - W_A \quad (5)$$

$$P_{BA} = 1 - P_{BB} \quad (6)$$

$$P_{AB} = (1 - W_A)/W_A \times (1 - P_{BB}) \quad (7)$$

$$P_{AA} = (2 \times W_A - 1)/W_A \times (1 - P_{BB}) \quad (8)$$

Plotting P_{AA} as a function of W_A, as proposed by Bethke *et al.* (1986), allows us to describe the whole range of possible stacking sequences for a two-component mixed layer with $S = 1$ (Fig. 8). When $P_{AA} = 1$ whatever the relative proportion of A layers, A and B layers are present in different crystals and this $P_{AA} = 1$ line corresponds to the physical mixture of periodic A and B phases. The opposite end of the diagram is defined by $P_{BB} = 0$ when $W_A > W_B$, meaning that it is impossible to find pairs of the minor layer. This corresponds to the maximum possible degree of ordering (MPDO) for $S = 1$. If $P_{BB} = 0$, then $P_{AA} = (2 \times W_A - 1)/W_A$ according to equation 8. The specific point of this line with $W_A = W_B = 0.5$ corresponds to the regular interstratification, or second staging, of A and B layers for which only ABAB ... sequences are allowed. Minerals corresponding to such regular interstratification exhibit a rational series of reflections ($d_{001} = l \times d_{00l}$) corresponding to the AB sequence (super-periodicity) and can be given names if the periodiocity is sufficient (Bailey *et al.*, 1982). The domain shown to the right of this curve on Figure 3 is prohibited as it would require negative values of the P_{BB} parameter. In Figure 8 it is also possible to recognize the $P_{AA} = W_A$ line, along which the probability of finding an A layer following another A layer (P_{AA}) is equal to the relative abundance of A layers in the mixed layer (W_A). In this specific case of $S = 1$, there is no influence of the nature of a given layer on the occurrence probability of the next one and the interstratification is thus random,

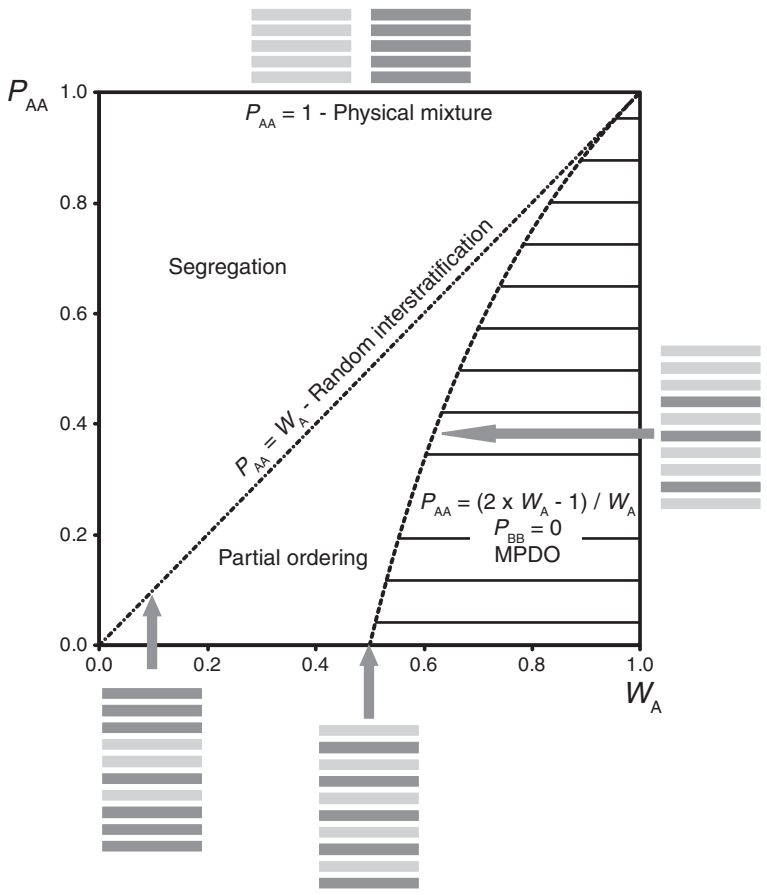

Fig. 8. Junction probability diagram for $S = 1$ two-component mixed layers (adapted from Bethke *et al.*, 1986). W_A and P_{AA} represent the relative proportion of A layers and the probability of finding an A layer after an A layer, respectively. Specific junction probabilities corresponding to random interstratification ($S = 0$) and maximum possible degree of ordering (MPDO) are shown as dotted-dashed and dashed lines, respectively. Domains corresponding to physical mixture, segregation and partial ordering are labelled. Possible stacking sequences corresponding to the different cases are schematized.

which is commonly described as the $S = 0$ case. The domains lying between physical mixture and random interstratification, on the one hand, and between random interstratification and maximum possible degree of ordering, on the other hand, are the domains of segregation and partial ordering, respectively. In the first domain, the presence of pairs of the minor layer is favoured ($1 > P_{AA} > W_A$ when $W_A < 0.5$), whereas this presence is hindered in the partial ordering domain ($0 < P_{AA} < W_A$ when $W_A < 0.5$), and prohibited ($P_{AA} = 0$) along the MPDO line. The relative proportions of the different stacking sequences, which are described by junction probability parameters, have an essential influence on diffraction patterns calculated for a given

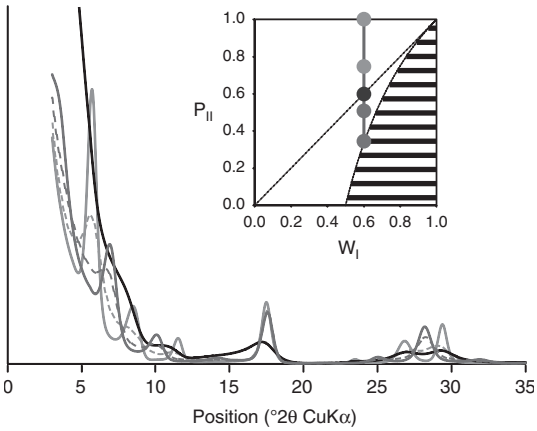

Fig. 9. XRD patterns calculated for the interstratification of illite and smectite layers as a function of junction probability parameters. Mixed-layer composition is constant ($W_I = 0.60$). Physical mixture ($P_{II} = 1.00$), segregation ($P_{II} = 0.733$), random interstratification ($P_{II} = 0.60$), partial ordering ($P_{II} = 0.50$), and MPDO ($P_{SS} = 0.00$, $P_{II} = 0.333$) cases are shown respectively as solid orange, dashed orange, solid black, dashed blue, and solid blue lines. The inset shows, in a diagram similar to Figure 8, the composition of the calculated mixed layer as a solid red line. Dots represent specific values of junction probability parameter P_{II} for which calculations were performed. Readers of the paper version of this chapter may wish to download a colour version of this figure from www.minersoc.org/emu-notes/emu-11/11-4-colour.pdf.

composition (relative proportions of the different layer types) and Reichweite parameter (Fig. 9). Occurrence and junction probability parameters are thus essential components of the structure model and should be reported as such (Bailey *et al.*, 1982; Guggenheim *et al.*, 2006).

This description provides a brief overview of the essential concepts and terms required for the description of stacking sequences in mixed layers and in lamellar compounds with well defined stacking faults. It should be noted however that the simplified view of stacking sequences offered by Figure 8 is hardly transposable for longer-range ($S > 1$) interactions that require first the definition of junction probability parameters describing the short-range ($S = 1$) order, which does not necessarily correspond to the MPDO case. Similarly, the description of multi-component mixed layers requires the definition of additional probability parameters. A more complete, although not comprehensive, description of occurrence and junction probability parameters can be found in Reynolds (1980) and Drits & Tchoubar (1990).

2.3.2. Usual identification methods

In the middle of the 20th century, Jacques Méring proposed theoretical developments allowing the prediction of diffraction effects arising from the random interstratification of layers having different basal spacings (Méring, 1949). According to that author, basal reflections corresponding to a randomly interstratified mixed layer (two-component) are located between neighbouring 00*l* reflections corresponding to periodic structures whose layers are interstratified. The actual position of these reflections depends on the relative proportions of the interstratified layer types, and on the respective intensity of the neighbouring 00*l* reflections. In addition, the breadth of the mixed-layer reflections increases with the 'distance' between the 00*l* reflections corresponding to periodic structures whose layers are interstratified ('Q-rule' of Moore & Reynolds, 1997). More generally, positions of basal reflections corresponding to an ordered A-rich A-B with

$S = 1$ or $S = 2$ are located between neighbouring 00*l* reflections corresponding to periodic stacking sequences consisting of A and AB ($S = 1$), or AAB ($S = 2$), fragments (Drits *et al.*, 1994). More recently, Drits & McCarty (1996) showed that the so-called 'Méring's rules' can be extended to predict the positions of non-basal reflections arising from randomly interstratified two-component systems consisting of layers having identical thicknesses. They showed, in particular, that non-basal reflections from such mixed layers are located between the nearest *hkl* reflections of the periodic phases whose fragments are interstratified, the actual position of these non-basal reflections depending on the relative proportions of interstratified fragments.

The predicted shift of peak position as a function of the actual composition of the mixed layer has allowed the development of simplified identification for commonly reported mixed layers. In natural environments, interstratification is especially widespread among clay minerals (phyllosilicates) which differ in the type of interstratified layers and in their stacking sequences. Because of the reactivity of the frequently interstratified expandable layers and of their resulting ability to evolve as a function of physicochemical conditions, these mixed layers have drawn special attention for decades in an effort to use them as indicators of palaeo-temperature conditions and/or of reaction progress (Hower & Mowatt, 1966; Perry & Hower, 1970; Lanson *et al.*, 2009). Several simplified methods have thus been proposed over the years for the identification of illite-smectite (Środoń, 1980, 1984; Watanabe, 1981, 1988; Velde *et al.*, 1986; Inoue *et al.*, 1989; Drits & Plançon, 1994; Drits *et al.*, 1994; Plançon & Drits, 1994, 2000). These methods rely essentially on peak-migration curves linking the position of a given reflection (or of a given set of reflections) to the composition (relative proportion of the different layer types) of the mixed layers. The curves were derived essentially from the calculation of XRD patterns using either *Newmod*, developed by Reynolds, or the program based on the matrix formalism developed by Watanabe. The intensity ratio between some of these reflections, or between reflections and 'background', is used occasionally as an additional criterion to estimate the relative contents of the different layer types in the mixed layers.

Despite their widespread use, these simplified identification methods have major drawbacks. The first is the lack of direct comparison between experimental and calculated patterns, which is intrinsic to the approach. As a result, there is no way to assess the validity of the identification by using a parameter measuring the 'goodness of fit' as is usual in structural studies. Direct comparison of experimental XRD patterns with those calculated on the basis of the identification performed allows us to refute peak position as a valid criterion for mixed-layers structure characterization (Claret *et al.*, 2004; McCarty *et al.*, 2008), and thus these simplified identification methods. Another drawback of these methods comes from the use of a unique XRD pattern for identification purposes, which does not allow the validation of the proposed identification by independent XRD measurements on the same sample submitted to different treatments (see section 2.3.3 on the description of the multi-specimen method).

In addition, the profiles of the diffraction lines, which are strongly affected by interstratification effects, are not taken into account by these peak-position methods. Other drawbacks are the limitations of the programs used to calculate diffraction effects

arising from mixed layers, and the limited range used for variable parameters in order to (over)simplify the identification process. Intrinsic limitations of the programs include, for example, their inability to calculate diffraction effects from multi-component mixed layers. Essential adjustable parameters which are insufficiently varied include the size and distribution of the coherent scattering domains, as the calculations are most often restricted to a single mean value, and junction probabilities. Most methods include calculations only for randomly interstratified mixed layers ($S = 0$, $P_{ii} = W_i$) and for the sole MPDO case for higher values of the Reichweite parameter, S, despite the key role of junction probabilities in the profiles of XRD patterns calculated for mixed layers (Fig. 9).

2.3.3. Multi-specimen method for XRD identification of mixed layers

Compared to usual structure determination and refinement methods, occurrence and junction probability parameters represent additional variable parameters required to describe the non-periodicity of stacking sequences. The quantitative comparison between experimental diffraction patterns and those calculated for the proposed structure model should thus be considered as a minimum requirement for the validation of this model in the case of mixed layers or of lamellar compounds exhibiting stacking faults. As the number of adjustable parameters is actually increased compared to periodic structures, it is valuable to consider additional constraints to the structure model.

These constraints are especially useful because of the low sensitivity of diffraction to the actual nature of structural disorder as illustrated by the common possibility of fitting the data equally well with different structure models (Drits, 1985). Experimental XRD patterns reported in Figure 10 are commonly attributed to randomly interstratified illite-smectite ($S = 0$, $W_S > W_I$) with a set of strong reflections whose positions are consistent with those of smectites, both in air-dried state (AD) and following ethylene-glycol solvation (EG), and a high low-angle shoulder for the 001 smectite peak (Inoue *et al.*, 1989). McCarty *et al.* (2009) and Lanson *et al.* (2009) reported that such XRD patterns could be described equally well assuming two distinct structure models (Fig. 10). The first assumes an illite-smectite in which smectite layers, the hydration and expansion behaviour of which is systematically heterogeneous, prevail. Junction probability parameters of this short-range ($S = 1$) mixed layer indicate the segregation of expandable layers ($P_{Exp\text{-}Exp} > W_{Exp}$). According to the alternative model, XRD patterns instead correspond to the physical mixture of discrete smectite, exhibiting again an heterogeneous hydration and expansion behaviour, and of a randomly interstratified illite-smectite in which illite layers prevail ($W_I > W_{Exp}$). Although the fit quality is improved slightly when using the mixture model (Lanson *et al.*, 2009), the two models provide satisfactory fits to the data, both in AD- and EG-solvated states (Fig. 10).

This example illustrates the need for (1) a quantitative comparison of XRD data with calculated patterns, and (2) additional constraints to assess the validity of structure models. Within this scope, and in contrast to most usual mixed-layer identification methods, the multi-specimen method requires the recording of XRD patterns for each sample after different treatments (*e.g.* Ca-saturated in AD- and/or EG-solvated states, and/or Na-saturated in AD-and/or EG-solvated states). For a given sample, XRD patterns

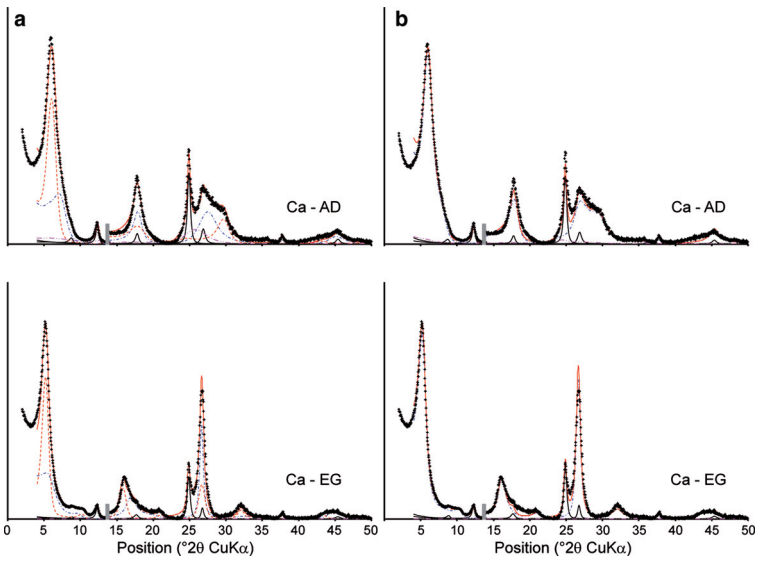

Fig. 10. Comparison between experimental and calculated XRD patterns for a diagenetically altered clayey sample from the Gulf Coast (adapted from Lanson *et al.*, 2009). XRD patterns were collected on Ca-saturated samples either air-dried and equilibrated at 40% relative humidity (Ca-AD – top) or solvated with ethylene glycol (Ca-EG – bottom). The grey bar indicates a modified scale factor for the high-angle region. (***a***) The structure model includes a randomly interstratified illite-smectite (57:43 ratio) and discrete smectite (dotted-dashed blue line and dashed red line, respectively) in addition to a randomly interstratified kaolinite-smectite (purple line), discrete kaolinite and discrete illite. (***b***) The structure model includes illite-smectite (45:55 ratio) with a tendency to segregation (dotted-dashed blue line) in addition to a randomly interstratified kaolinite-smectite (purple line), discrete kaolinite and discrete illite. Readers of the paper version of this chapter may wish to download a colour version of this figure from www.minersoc.org/emu-notes/emu-11/11-4-colour.pdf.

usually differ significantly after these treatments owing to the contrasting hydration/expansion properties of expandable layers. It is then possible to extract additional constraints on the actual structure of the different minerals present.

The method itself was proposed initially by Drits *et al.* (1997) and Sakharov *et al.* (1999a, 1999b), and consists of direct comparison of experimental XRD profiles with those calculated for a structure model. The optimum agreement between experimental and calculated XRD patterns is obtained by a trial-and-error procedure. Structure models include for each mixed layer, the number (not limited to 2), the nature and proportions of the different layer types and a statistical description of their stacking sequences (Reichweite parameter and junction probabilities). The different treatments may change the thickness and the scattering power (nature, amount and position of interlayer species) of the expandable interlayers but not the distribution of the different layer types. A consistent structure model is thus obtained for one sample when the stacking sequences of the different layer types obtained from all experimental XRD profiles of the same sample are nearly identical. In addition to these structural parameters,

relative contributions of the various phases (including mixed layers) to the different XRD patterns recorded for the same sample must be similar for polyphasic clay parageneses (Sakharov *et al.*, 1999a; Claret *et al.*, 2004).

By constraining the structural characterization of a given sample from different experimental XRD patterns, the multi-specimen method allows us to overcome one major intrinsic limitation of the XRD identification of clay minerals. This limitation arises from the strong tendency of XRD to average structural parameters describing the periodicity of crystals. The resulting low sensitivity of XRD to variation in local disorder can allow for the possibility of several structure models giving rise to similar diffraction effects for a given set of experimental conditions. To determine the actual structure model, additional constraints obtained from the analysis of different XRD patterns obtained from the same sample after different treatments are thus essential (Sakharov *et al.*, 1999a; McCarty *et al.*, 2004). In addition, this method allows for a semi-quantitative phase analysis of the clay fraction including both discrete and mixed-layer clay phases in addition to the detailed structural characterization of these different components.

3. Structural characterization of defective layered structures

In the following sections, a variety of examples from the recent literature, in which defective lamellar compounds have been reported and/or the structure of which has been determined, is reviewed. Studies where the structure model was checked against the data have been favoured in the selection process required by the large number of examples available. Emphasis was placed on the variety of structural parameters required for a thorough and realistic description of their actual structure. The first objective of this review is to illustrate the potential of the different approaches for the structural characterization of non-periodic compounds. Limitations of the different approaches will also be assessed.

3.1. Layered silicates: structural characterization of mixed layers the elementary layers of which differ from their basal spacings

3.1.1. Layered silicates: hydration and expansion heterogeneity, intercalation

Because of their ability to incorporate and to exchange a variety of cations and molecules in their interlayer spaces, layers having different basal distances often coexist in expandable layered silicates (smectites), despite the overall homogeneity of layer charge. For example, Méring & Glaeser (1954) reported the interstratification of smectite layers with contrasting interlayer cation contents resulting from a partial exchange of Na by Ca. The random interstratification of Ca- and Na-saturated smectites was particularly visible under low relative humidity (RH) conditions from peak positions intermediate between those characteristic of the two end-members. At 5% RH, Na-saturated smectite was indeed dehydrated (0W smectite – $d_{001} \approx 9.6$ Å) whereas Ca-saturated interlayers incorporate a unique plane of H_2O molecules (monohydrated, or 1W, smectites – $d_{001} \approx 12.4$ Å).

The contrasting hydration energy of alkali and alkaline earth cations result, for a given RH value, in different hydration states for smectite layers depending on the interlayer cation. This specific behaviour allows us, for example, to prove the coexistence of different cations in smectite interlayers if the hydration contrast and/or the interlayer electronic density contrast is sufficient (Iwasaki & Watanabe, 1988; Ferrage *et al.*, 2005d). These authors used such a model to demonstrate that within a given interlayer, all cations are exchanged at the same time, leading to the segregation of the different cations in different interlayers. As a result, diffraction patterns indicate the interstratification of layer types whose contrasting hydration, and thus basal spacing, is characteristic of their cationic content. Oueslati *et al.* (2009) used a similar approach to assess the selectivity of smectite for different cations as a function of the ionic strength. In smectite samples saturated with bi-cationic solutions, they determined the relative proportion of mono- and divalent cations from the modelling of XRD patterns, each cation being characterized by its specific hydration behaviour. They deduced that at low ionic strength, smectites favour the presence of cations with low hydration over more hydrated cations.

Interstratification of smectite layers exhibiting different hydration states was reported also in homoionic smectite (Méring & Glaeser, 1954; Walker, 1956; Glaeser *et al.*, 1967; Sato *et al.*, 1992, 1996). More recently, the potential of smectite interlayer water as a vector for the migration of contaminants (*e.g.* radionuclides) or as a water 'reservoir' in deep geological formations has renewed the interest in its study. In particular, smectite hydration has been thoroughly described as a function of (1) the relative humidity under ambient pressure and temperature conditions, (2) the amount and location of layer charge, (3) the interlayer cation (Bérend *et al.*, 1995; Cases *et al.*, 1997; Calarge *et al.*, 2003; Meunier *et al.*, 2004). Ferrage *et al.* (2005a, 2005b, 2007c, 2010) and Karmous *et al.* (2009) showed that heterogeneity, rather than homogeneity, is the rule for smectite hydration even for homoionic specimens under controlled RH conditions. For such samples, these authors showed the systematic interstratification of layer types exhibiting contrasting hydration states. Moreover, the contributions of various randomly interstratified mixed layers are commonly required to account for the sample heterogeneity (Fig. 11). Although these contributions do not imply the actual presence of distinct (sub-)populations of particles in the sample, they indicate the partial segregation of the different hydration states within the sample.

A similar modelling approach could be implemented for a variety of samples in order to understand, for example, the link between smectite hydration and the amount and location of charge deficit. Ferrage *et al.* (2005b, 2007c) and Karmous *et al.* (2009) performed such a study on di- and trioctahedral smectites, respectively, suggesting in both cases the increased hydration heterogeneity in tetrahedrally substituted smectites. Ferrage *et al.* (2005b, 2007c) also proposed a conceptual model to reconcile the greater hydration of smectite, as estimated from the number of interlayer H_2O molecules, when increasing the layer charge deficit and the associated lower value of the basal distance. In a remarkable effort to overcome the intrinsic time-consuming character of the trial-and-error approach, Ferrage *et al.* (2007a) modelled hundreds of XRD traces obtained *in situ* while dehydrating smectite at different temperatures. The relative

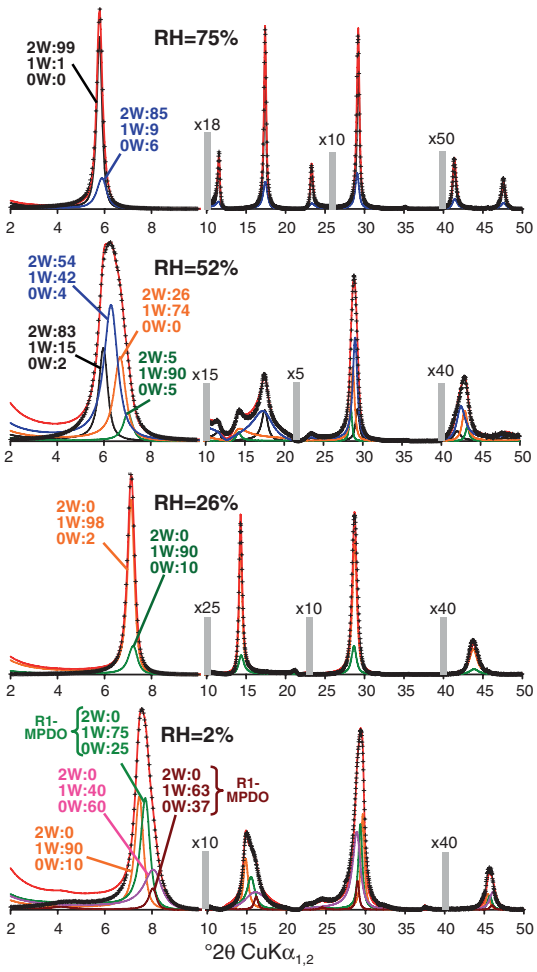

Fig. 11. Comparison between experimental and calculated XRD patterns as a function of RH for a low-charge saponite (trioctahedral smectite – adapted from Ferrage *et al.*, 2010). Respective contributions of the various mixed layers to the calculated profiles are shown in different colours. Experimental and calculated XRD patterns are shown as crosses and solid red lines, respectively. Other symbols as in Figure 10. Readers of the paper version of this chapter may wish to download a colour version of this figure from www.minersoc.org/emu-notes/emu-11/11-4-colour.pdf.

proportions of the different hydration states were thus determined as a function of temperature and dehydration time and served as the basis for the derivation of smectite dehydration kinetic parameters (Ferrage *et al.*, 2007b).

In most of the studies described above, interstratification of smectite layers with different cation content or hydration is essentially random, thus supporting the assertion that 'spontaneous segregation of diverse guest species into separate but stacked interlayers by a process comparable to staged heterostructures in graphite is rare' (Ijdo *et al.*, 1996). Walker (1956) reported, however, the ordered interstratification of 0W and 1W smectites layers from the presence of a 20.6 Å (9.0 + 11.6 Å) superperiodicity exhibiting >20 reflections as evidence of the high degree of regularity of the mixed layer. Additional reports of such ordered interstratification of smectite layers with different hydration states commonly describe this phenomenon as affecting only a minor part of the sample with much reduced regularity, at least for natural samples (Moore & Hower, 1986; Chipera & Bish, 2001; Ferrage *et al.*, 2007c).

Regular alternation, or interstratification, of organic and inorganic interlayer cations was, however, achieved successfully in an effort to prepare materials with amphiphilic properties from smectites (Ijdo & Pinnavaia, 1998a, 1998b). Second staging was identified from the presence of a reflection corresponding to the 1:1 regular interstratification ($S = 1$, MPDO) of layers with sodium and alkylammonium interlayer cations as a result of the partial exchange of sodium. Such regular interstratification was also achieved with a synthetic

smectite for different inorganic cations having contrasting hydration energies (Möller *et al.*, 2010a, 2010b). In both cases, the regular interstratification probably originates from the increased charge homogeneity of the synthetic smectites used compared to natural varieties. Charge homogeneity favours the alternation of cations with different hydration properties in successive interlayers to optimize local charge compensation. Möller *et al.* (2010b) actually hypothesized, from ^{23}Na magic angle spinning nuclear magnetic resonance (MAS NMR) spectroscopy data, different contents of interlayer cations in successive interlayers despite the remarkably homogeneous layer-charge distribution (Breu *et al.*, 2001).

3.1.2. Natural occurrence of multi-component mixed layers

Even though mixed layers containing more than two layer types have been described only recently in the wealth of literature devoted to the structural characterization of these minerals, such multi-component (3- but also 4-component) mixed layers are most likely overwhelmingly present, and more especially so in natural samples. Heterogeneity rather than homogeneity is the rule for smectite hydration and expandability, even when working with homoionic samples under controlled RH conditions. Although "it is not certain that single layers of smectite or of vermiculite sandwiched between layers of a different type in an interstratification react in the same way as the non-interstratified minerals would react to solvation, hydration, and dehydration tests" (Bailey *et al.*, 1982), heterogeneity is probably common in mixed layers implying expandable layers. Consistently, all recent studies performed with calculation algorithms allowing the calculation of their XRD patterns have led to the identification of mixed layers that include more than two components as the result of the systematic heterogeneity of the swelling/hydration behaviour of expandable layers (Drits *et al.*, 1997, 2002a, 2002b, 2004, 2007b; Sakharov *et al.*, 1999a, 1999b, 2004a; Lindgreen *et al.*, 2000, 2002, 2008; Claret *et al.*, 2004; McCarty *et al.*, 2004, 2008; Inoue *et al.*, 2005; Aplin *et al.*, 2006; Hubert *et al.*, 2009; Lanson *et al.*, 2009). It should be noted that heterogeneity is systematically present whatever the chemistry (both Fe- and Al-rich) of expandable layers (McCarty *et al.*, 2004). In addition, hydration behaviour exhibited by expandable layers in smectite is not restricted to the usual 0W (d_{001} = 9.6–10.0 Å), 1W (d_{001} = 12.0–12.8 Å), and 2W (d_{001} = 14.8–15.6 Å) states and 'unusual' basal spacings have been reported for hydrated expandable layers (*e.g.* Lindgreen *et al.*, 2002; Lanson *et al.*, 2009; Fig. 12) as suggested by Bailey *et al.* (1982). This heterogeneity evidently proscribes the use of simplified peak-migration methods for the identification of mixed layers. Heterogeneity is actually not restricted to expandable layers, and the coexistence of different mica-like layers in a given mixed layer has also been reported, thus reinforcing the inability of these methods to provide a satisfactory identification of mixed layers. In particular, the coexistence of K^+ and NH_4^+ has been demonstrated repeatedly in the context of burial diagenesis in the vicinity of source rocks (Sakharov *et al.*, 1999a; Lindgreen *et al.*, 2000; Drits *et al.*, 2001, 2002a, 2005, 2007b).

In addition to the mixed layers whose multi-component character originates from the heterogeneity of the expandable or micaceous layers, mixed layers containing three really distinct layer types have been reported. In particular, complex mixed layers

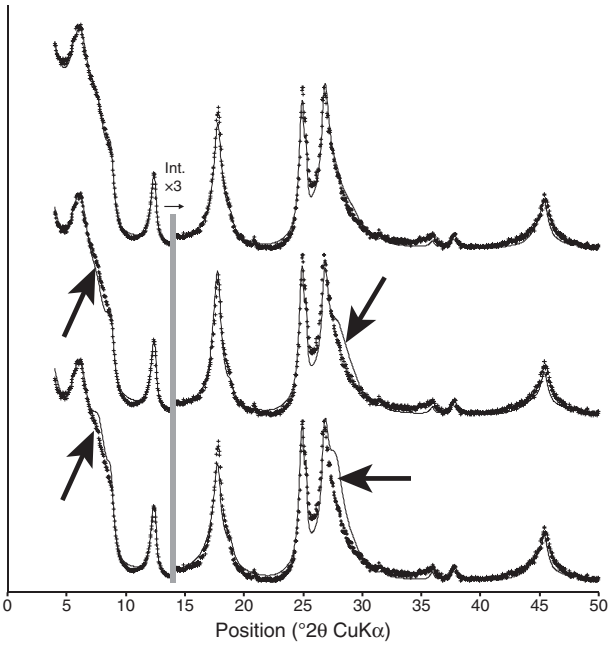

Fig. 12. Comparison between experimental and calculated XRD patterns for a diagenetically altered clayey sample from the Gulf Coast (adapted from Lanson *et al.*, 2009). XRD patterns were collected on Ca-saturated samples air-dried and equilibrated at 40% relative humidity. In addition to discrete illite, kaolinite, smectite, and chlorite, the optimum structure model includes a randomly interstratified kaolinite-smectite and a randomly interstratified illite-smectite (62:38 ratio). From top to bottom, the relative proportion of 15.00, 14.00, and 12.50 Å expandable layers in the latter mixed layer are 15:8:15 (optimum values), 23:0:15 and 15:0:23. Symbols as in Figure 10.

involving the coexistence of illite and expandable layers together with dioctahedral chlorite (sudoite) layers, seldom described as a discrete phase, have been described repeatedly especially in the context of burial diagenesis of clayey sediments (Lindgreen *et al.*, 2002, 2008; Lanson *et al.*, 2009) but also in soils (Hubert *et al.*, 2011). The interstratification of illite and expandable layers with kaolinite, rather than chlorite, layers has also been reported in a burial-diagenesis context (Drits *et al.*, 1997; Sakharov *et al.*, 1999b). More seldom-described complex mixed layers include berthierine-chlorite-smectite (McCarty *et al.*, 2004) and mica-pyrophyllite-smectite (Drits *et al.*, 2007b).

A variety of mixed layers other than those listed above has been reported over the last decade or so. Interstratification of chorite and expandable layers has, for example, been described both in superficial (Hubert *et al.*, 2009) and deep environments (Lindgreen *et al.*, 2002). Beaufort *et al.* (1997) challenged the commonly accepted description of the saponite-to-chlorite conversion series reporting the existence of chlorite-corrensite, both from XRD data and lattice-fringe images obtained under the transmission electron microscope (TEM). Chlorite layers can also be interstratified with 1:1 phyllosilicates (serpentine – Drits *et al.*, 2001, 2007b; Lindgreen *et al.*, 2002; McCarty *et al.*, 2004). Serpentine layers are usually required to fit the increased breadth of odd order chlorite reflections, compared to even ones, and their relative low intensities compared to the ideal intensity distribution calculated for a periodic chlorite with the correct composition (Moore & Reynolds, 1997; Drits *et al.*, 2001). Kaolinite-smectite (Sakharov & Drits, 1973; Sudo & Shimoda, 1977; Brindley *et al.*, 1983; McCarty *et al.*, 2004; Lanson

et al., 2009), serpentine-smectite (Sakharov *et al.*, 2004a), illite-chlorite (Hubert *et al.*, 2011), and illite-kaolinite (Hubert *et al.*, 2011) have also been reported.

3.1.3. Additional complexity of naturally occurring mixed layers

Using a whole-pattern profile-modelling approach, such as the multi-specimen approach, rather than the position of the main diffraction lines to determine the clay paragenesis allowed the uncovering of their frequent polyphasic character. Various mixed layers are indeed frequently reported as coexisting with discrete phases (Drits *et al.*, 1997, 2002a, 2002b, 2004, 2007b; Sakharov *et al.*, 1999a, 1999b; Lindgreen *et al.*, 2002, 2008; Claret *et al.*, 2004; McCarty *et al.*, 2004, 2008, 2009; Aplin *et al.*, 2006; Hubert *et al.*, 2009; Lanson *et al.*, 2009; Ferrage *et al.*, 2011b). Two major factors contribute to this recently revealed mineralogical complexity. The first is the coexistence of mixed layers having similar although distinct compositions or ordering parameters owing to the kinetics of clay mineral (trans)formation processes at low temperature. The coexistence of such mixed layers, whose contributions to the diffracted intensity are closely related, modifies the reflection profiles, and more especially their low-intensity side tails. In particular, mixed layers that do not contribute to any of the well defined maxima can be overlooked completely (Fig. 13). The second factor, which is not necessarily separate from the first, is the frequent presence of mixed layers characterized by broad and poorly defined contributions to the diffracted intensity, especially in the low-angle region (Fig. 13). Careful XRD profile fitting has, for example, allowed us to reveal the frequent presence of randomly interstratified illite-smectite with a high illite content (60–70% illite) in diagenetically altered sediments, soils, *etc.* (Claret *et al.*, 2004; Lanson *et al.*, 2005, 2009; Aplin *et al.*, 2006; Lindgreen *et al.*, 2008; McCarty *et al.*, 2008, 2009; Hubert *et al.*, 2009). The specific diffraction fingerprint, without a significant maximum in the low-angle region (Fig. 13), probably hinders recognition of such highly illitic randomly interstratified mixed layers in natural samples and is probably responsible for the small number of descriptions in works based on the position of diffraction maxima.

In addition, the existence of partial segregation, or partial ordering, has frequently been reported in studies of natural and synthetic mixed layers performed with the multi-specimen method (Drits *et al.*, 1997, 2002b, 2004; Sakharov *et al.*, 1999a, 1999b; Claret *et al.*, 2004; Inoue *et al.*, 2005; McCarty *et al.*, 2008, 2009; Hubert *et al.*, 2009, 2011; Lanson *et al.*, 2009; Ferrage *et al.*, 2011b). The high frequency of natural mixed layers exhibiting junction probabilities different from the usual $S = 0$ and $S = 1$ for MPDO cases clearly demonstrates that XRD profile modelling is the one tool that can provide an accurate structure characterization of mixed layers as peak migration curves are not available for junction probabilities different from these 'ideal' cases.

3.1.4. Recent developments and new insights into the actual structure of mixed layers: structure of elementary layers

Quantitative description of mixed-layer diffraction patterns, which has been used increasingly over the past decade, has not only allowed a more realistic description of mixed layers but has also brought significant new insights into the structure of individual

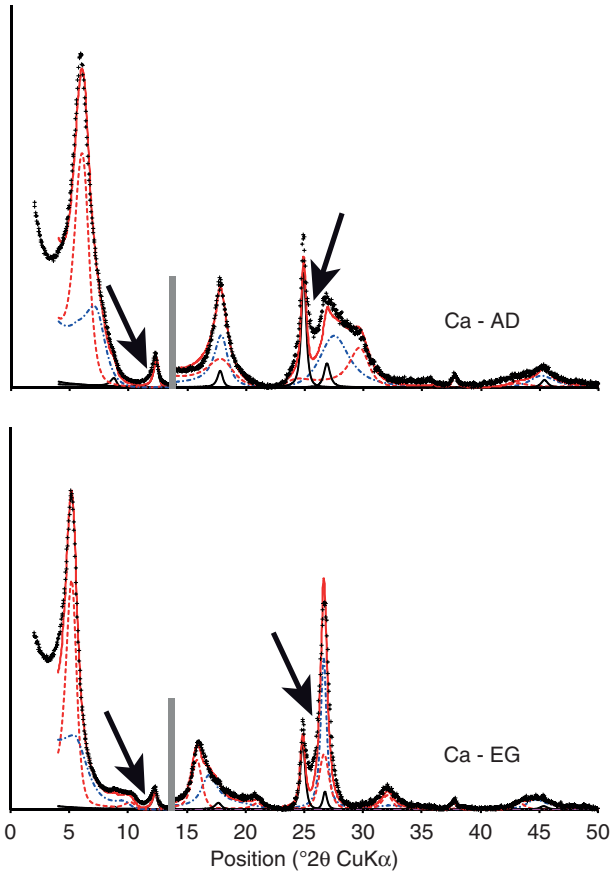

Fig. 13. Comparison between experimental and calculated XRD patterns for the diagenetically altered clayey sample from the Gulf Coast shown in Figure 10 (adapted from Lanson *et al.*, 2009). Unlike the optimum fit shown in Figure 10a, the contribution of the randomly interstratified kaolinite-smectite to the diffracted intensity has not been considered. Readers of the paper version of this chapter may wish to download a colour version of this figure from www.minersoc.org/emu-notes/emu-11/11-4-colour.pdf.

layers. For example, the structure description of interlayer H_2O in expandable layered silicates was improved, despite their intrinsic hydration heterogeneity. It was, in particular, possible to refute the widely used model with three planes of H_2O molecules on each side of the interlayer mid-plane reported by Moore & Reynolds (1997). Instead, a model with a single plane of H_2O molecules on each side of the interlayer mid-plane, which contains charge-compensating cations, was proposed (Ferrage *et al.*, 2005a, 2005b, 2010). Furthermore, it has been shown that the total number of H_2O molecules filling these planes is not constant but rather increases with increasing RH conditions. At the same time, the layer-to-layer distance, but also the distance – perpendicular to the layer plane – from the interlayer mid-plane to the plane of H_2O molecules, increases also to accommodate the larger number of H_2O molecules in the smectite interlayers. Finally, it was shown that thermal motion, commonly described as the Debye-Waller factor, accounted inadequately for the positional disorder of H_2O molecules about these planes. This disorder was better described with a Gaussian function, in agreement with previous models proposed for smectite interlayer H_2O (de la Calle *et al.*, 1977; Ben Brahim *et al.*, 1983; Slade *et al.*, 1985). This configuration allows reproduction of all 00*l* reflections with high precision, with only one new variable parameter (the width of the Gaussian function). In addition, the proposed configuration allows us to match more closely the

amount of interlayer water that can be determined independently from water-vapour adsorption/desorption isotherm experiments. Additional Monte Carlo simulations performed in the NVT (Ferrage *et al.*, 2005a) or μVT (Ferrage *et al.*, 2011a) ensembles further supported the proposed model. The combined modelling of X-ray and neutron diffraction data has even allowed us to assess the different sets of potential available in the literature for the clay layer; the *CLAYFF* model proposed by Cygan *et al.* (2004) was shown to account better for the water content and organization compared to the model developed by Skipper *et al.* (1995) and modified by Smith (1998). However, fitting diffraction data for bi-hydrated samples using *CLAYFF* simulations requires us to refine further Lennard-Jones parameters for oxygen atoms of the clay layer (Ferrage *et al.*, 2011a). When combined with the SPC/E water model, this modified version of *CLAYFF* allows matching of experimental water contents and fitting of the complete set of X-ray and neutron-diffraction data obtained on both mono- and bi-hydrated smectites (Fig. 14).

In addition to the distribution of interlayer species, XRD profile modelling has allowed the refinement of structural parameters such as the layer-to-layer distance corresponding to the different layer types for a variety of interlayer cations and a large range of RH values. It was also possible to show that for a given cation and RH value, the basal distance actually scatters about an average distance, and that accurate modelling of experimental data requires that we consider second-order fluctuations of the layer-to-layer distance (Ferrage *et al.*, 2005a, 2005b, 2010). These fluctuations are probably linked to the incomplete, and thus heterogeneous, filling of smectite interlayers (Fig. 15 – Ferrage *et al.*, 2005c). Experience has shown that even for complex mixtures

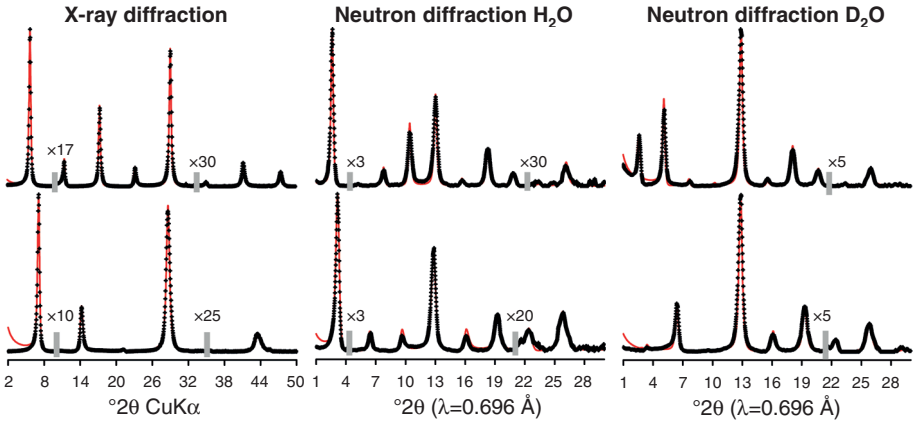

Fig. 14. Comparison between experimental and calculated diffraction patterns for the low-charge saponite shown in Figure 11 (adapted from Ferrage *et al.*, 2011a). The density profiles of interlayer species were derived from Monte-Carlo simulations performed in the Grand Canonical ensemble using a modified version of the CLAYFF model (modified Lennard-Jones parameters for oxygen atoms of the clay layer) and the SPC/E water model. Readers of the paper version of this chapter may wish to download a colour version of this figure from www.minersoc.org/emu-notes/emu-11/11-4-colour.pdf.

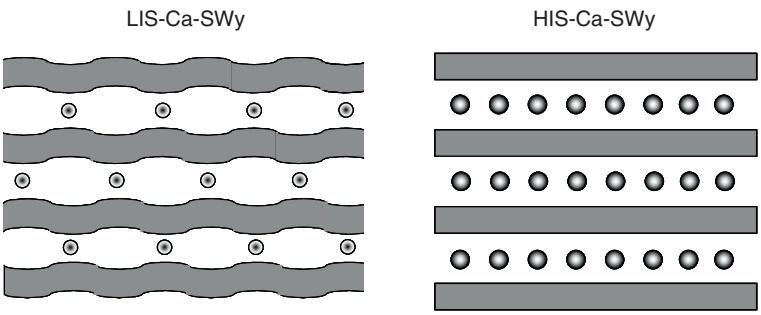

Fig. 15. Schematic representation of the influence of *Me*Cl^+ ion pairs on smectite interlayers (adapted from Ferrage *et al.*, 2005c). The incomplete interlayer filling of sample SWy Ca-saturated using low ionic strength solutions (left) leads to significant fluctuations of the layer-to-layer distance because of the local balance between attractive (between layer and interlayer cations) and repulsive (between adjacent layers) forces. For sample SWy Ca-saturated using high ionic strength solutions (right), the more complete filling of the interlayer space by $CaCl^+$ pairs leads both to an increased layer-to-layer distance and to a more homogeneous distribution of interlayer species, thus reducing the fluctuation of the layer-to-layer distance.

of natural mixed layers, the description of experimental data is significantly improved when such fluctuations are considered (Drits *et al.*, 1997, 2002b; Sakharov *et al.*, 1999a; Lindgreen *et al.*, 2000; Drits, 2003), although the parameter quantifying the extent of the fluctuation is not systematically reported.

3.1.5. Recent developments and new insights into the actual structure of mixed layers: intra-crystalline defects

Structure models of mixed layers used for the calculation of XRD profiles most often describe coherent scattering domains (CSDs) limited to a few layers. These models describe well the high-angle region of the experimental diffraction patterns but often fail over the low-angle region ($2\theta < 4-6^\circ$Cu$K\alpha$), where the calculated intensity is much greater than the experimental intensity. On the other hand, simulation of small-angle X-ray scattering data obtained on related samples commonly indicate the presence of much thicker CSDs (Pons *et al.*, 1981, 1982).

In an effort to reconcile the results from both methods, Plançon proposed a model for the simulation of experimental XRD patterns in which particles, or megacrystals, are significantly thicker than crystals (or CSDs) used in XRD models (Plançon, 2002). These particles contain layer types identical to those in the usual XRD model. Their relative proportion and their stacking sequences are also identical to those in the usual models. However, adjacent layers may be shifted with respect to each other along the c^* axis according to an adjustable probability. As a result, the apparent CSD size decreases with increasing 2θ angle and XRD patterns calculated according to this new model exhibit a significantly lower scattered intensity over the low-angle region compared to the usual XRD models.

However, this model leads to non-negligible discrepancies between the basal-reflection positions and intensities calculated in the high-angle region compared to usual XRD

models. To overcome this problem, an improved model describing the degree of coherency within megacrystals has been proposed (Sakharov, 2005). In contrast to the model proposed by Plançon, this model hypothesizes that CSDs are identical to the usual XRD models. In addition, within megacrystals, these CSDs may be shifted with respect to each other along the c^* axis according to an adjustable probability. This model allows reproduction of diffraction features in both high- and low-angle regions of experimental XRD patterns (McCarty *et al.*, 2009).

3.1.6. Recent developments and new insights into the actual structure of mixed layers: outer surfaces of crystals

None of the algorithms routinely available to simulate XRD patterns of mixed layers can account for the possibility that in natural environments the structure and composition of surface layers of crystals may differ from those of 'core' layers. However, knowledge of the nature of the outer surface layer (OSL) is helpful in understanding better the surface properties of mixed layers and/or to derive constraints on their growth conditions. For example, according to high-resolution TEM, illite crystals may terminate on a kaolinite layer (Tsipursky *et al.*, 1992) whereas kaolinite crystals may have pyrophyllite or smectite layers as surface terminations (Ma & Eggleton, 1999). Kogure *et al.* (2001) also reported crondstedtite crystals exhibiting chlorite OSLs.

Alternative algorithms were thus proposed that allow us to determine the nature of OSLs in mixed layers from the simulation of XRD patterns (Sakharov *et al.*, 1999c, 2004b; Plançon, 2003). In particular, Sakharov *et al.* (2004b) showed that among the usual mixed layers found in natural samples, most significant effects are calculated for those containing elementary chlorite layers. For chlorite samples, the relative intensities of the odd reflections depend not only on the distribution of Fe in the chlorite structure over the 2:1 and 0:1 layers, but also on the nature of the OSLs. For the two samples they investigated, brucite sheets were present on the outer crystal surfaces. However, comparison of the OSL nature determined from XRD profile modelling with that deduced from direct observations using electron or atomic force microscopies remains essential for mixed layers because similar diffraction effects may be obtained by varying the structural and chemical parameters of the mixed layers on the one hand and the OSL nature on the other.

Sakharov *et al.* (2004b) showed also that for periodic structures containing only one layer type, the influence of OSLs may be predicted from simple calculations, and is independent of the scattering power of the OSL. Such a prediction is not possible for mixed layers.

3.2. Natural layered silicates: interstratification of structural fragments differing in terms of their internal structure or their stacking mode

To complement the structural characterization of phyllosilicate expandable interlayers in projection along the c^* axis (see section 3.1.4), simulation of *hkl* reflections, or of *hk* bands, has been used to determine also the *x* and *y* coordinates of interlayer H_2O molecules. For example, Ben Brahim *et al.* (1984) performed such a study on bi-hydrated

beidellite. Despite the large proportion of random stacking faults (~70%), these authors determined the nature of the layer displacements, when not random, the occurrence probabilities of the different possible displacements, and the atomic coordinates of interlayer species. Similarly, Argüelles *et al.* (2010) refined simultaneously the layer displacement and the atomic coordinates of interlayer H_2O molecules in bi-hydrated vermiculite. The refined model includes the random alternation of $+b/3$ and $-b/3$ layer displacements, thus defining two layer types differing by their interlayer configuration and the position of their interlayer species. This model is fully consistent with that proposed by de la Calle *et al.* (1988) from the qualitative comparison of their data with XRD patterns calculated for a variety of structure models.

The actual layer stacking, and the nature of stacking defects, has also been determined in kaolinite from the calculation of the diffraction effects corresponding to different structure models. In particular, Plançon & Tchoubar (1977) used this approach to reject both rotational and $\pm b/3$ stacking faults as possible defects in kaolinite. Rather, these authors proposed that stacking defects in kaolinite correspond to the different location of the vacant octahedral layer site in successive layers among the three non-equivalent (A, B, or C) sites. Bookin *et al.* (1989) and Drits & Tchoubar (1990) improved this model and showed that kaolinite is composed only of B layers that can actually present two stacking vectors within the *ab* plane: $\mathbf{t}_1$ (-0.369 $\mathbf{a}_1$, -0.024 $\mathbf{b}_1$) and $\mathbf{t}_2$ (-0.352 $\mathbf{a}_1$, $+0.304$ $\mathbf{b}_1$), corresponding to right- and left-handed kaolinite unit cells. Plançon *et al.* (1989) validated this model by fitting the XRD data obtained from kaolinite samples exhibiting a wide range of structural imperfection.

Recently, this model was validated further by the direct imaging, using high-resolution TEM (HRTEM), of the layer structure and stacking in kaolinite (Kogure & Inoue, 2005). In particular, these authors described the occurrence of $\mathbf{t}_1$, $\mathbf{t}_2$ and $\mathbf{t}_0$ ($\sim -a_1/3$, $\sim -b_1/3$) layer displacements and the sole presence of B layers. Kogure *et al.* (2010) observed also $\mathbf{t}_1$ and $\mathbf{t}_2$ layer displacements between successive kaolinite layers. These two well defined stacking vectors occur either as isolated faults (for example a $\mathbf{t}_2$ layer displacement within an ordered sequence characterized by a $\mathbf{t}_1$ vector), or as the alternation of multilayer ordered blocks with either $\mathbf{t}_1$ or $\mathbf{t}_2$ vectors (segregated mixed layer). The combination of diffraction effects arising from these two types of defects allows us to reproduce, at least qualitatively, XRD intensities recorded for the investigated sample. It was also possible, using HRTEM, to reject the interstratification of kaolinite (sequence of B layers only) and of dickite (BC sequence of layers) fragments in samples from a diagenetic kaolinite-to-dickite transition series (Kameda *et al.*, 2008).

Stacking disorder was characterized in other dioctahedral phyllosilicates by coupling direct HRTEM imaging of stacking and calculation of diffraction effects from the observed stacking faults. In both sudoite (Kameda *et al.*, 2007) and pyrophyllite (Kogure *et al.*, 2006b; Kogure & Kameda, 2008), stacking disorder is, as in kaolinite, essentially induced by the coexistence of two possible layer displacements (Fig. 16). Contrastingly, stacking faults in trioctahedral phyllosilicates are related mainly to rotations between successive 2:1 layers (Kogure *et al.*, 2006b; Kogure & Kameda, 2008). The contrast between di- and trioctahedral varieties was tentatively attributed

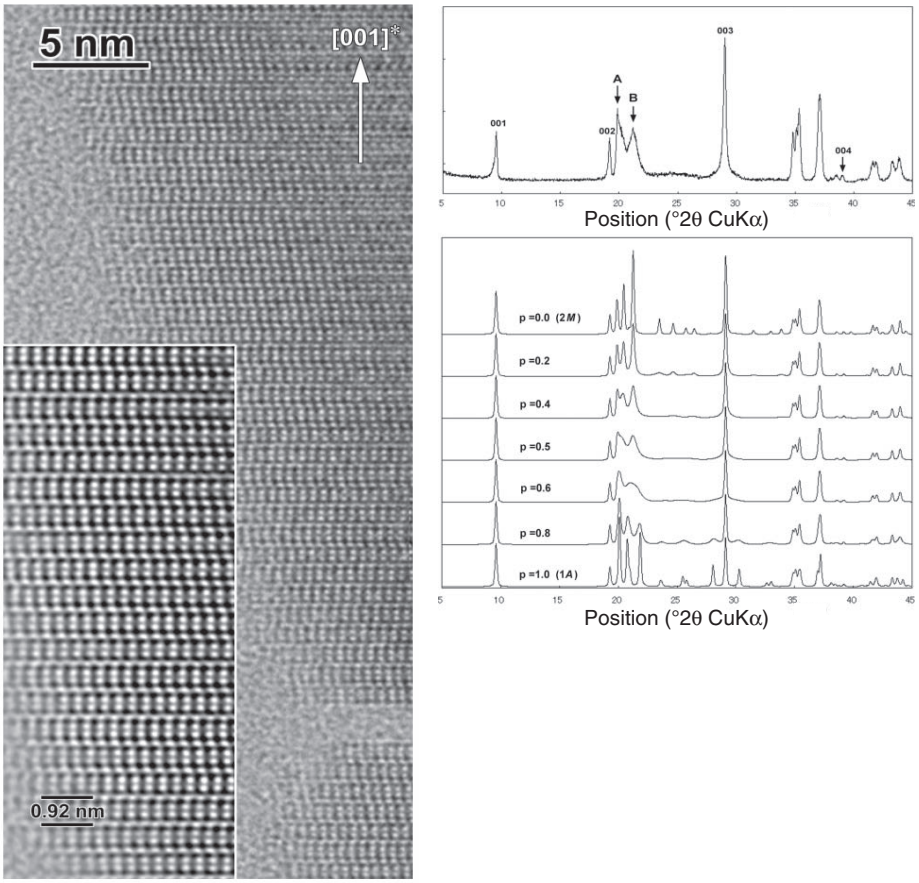

Fig. 16. (left) HRTEM image of the Berozovska pyrophyllite (adapted from Kogure *et al.*, 2006a). The inset at the bottom-left is a filtered and magnified portion of the main image. The contrast for each 2:1 layer is uniform but the direction of shift between adjacent layers is near perfectly disordered. (right) Powder XRD pattern of Nowa pyrophyllite (top) and powder XRD patterns calculated for variable proportions of stacking faults identified on HRTEM images (bottom – adapted from Kogure & Kameda, 2008).

to the corrugation of basal oxygen planes in dioctahedral varieties, although rotational stacking faults were also reported in the dioctahedral mica, celadonite (Kogure *et al.*, 2008).

Reynolds (1993) and McCarty & Reynolds (1995) described the presence of rotational stacking faults in the dioctahedral mica, illite. Simultaneously, these authors determined the internal structure of dioctahedral layered silicates, and more especially the distribution of the layer vacancy between non-equivalent *cis* and *trans* sites. In addition to the modification of the intensity distribution between the different *hkl* reflections, *cis*- and *trans*-vacant dioctahedral micas are characterized by different layer displacements allowing diffraction effects similar to those observed for the

interstratification of layers having different layer thickness (see section 2.3.2.). Extending Méring's principle to 3D structures, Drits & McCarty (1996) and Drits *et al.* (1998b) proposed and validated a method, based on peak-migration curves, to obtain a semi-quantitative (and quick) estimate of *cis*- and *trans*-vacant polymorphs in illite and illite-smectite. From systematic calculations of diffraction effects, Drits & Sakharov (2004) demonstrated that the coexistence of *cis*- and *trans*-vacant layers may significantly modify the intensity distribution between the different *hkl* reflections and thus the identification of mica polytypes.

A similar variability of the octahedral cation distribution over *cis* and *trans* sites has been reported in glauconites (Drits *et al.*, 2010), pyrophyllite (Drits *et al.*, 2011), and dioctahedral smectites (Tsipursky & Drits, 1984; Emmerich *et al.*, 2009). A similar fitting of XRD data may be used to unravel this distribution in smectites pending an improvement of their stacking order obtained by the saturation of interlayers with large anhydrous cations (K^+, Cs^+) and subsequent wetting-and-drying cycles (Besson *et al.*, 1983; Tsipursky & Drits, 1984; Cuadros, 2002). It is clear that a comprehensive structural characterization of dioctahedral phyllosilicates should include the description of this distribution, which in turn could provide key information on their (trans)formation mechanisms (Drits & Zviagina, 2009; McCarty *et al.*, 2009).

3.3. Interstratification of other lamellar structures: layered double hydroxides

Layered double hydroxides (LDHs) form a large family of promising materials, natural and synthetic, that can be used as catalysts (Cavani *et al.*, 1991), catalyst supports (Vaccari, 1998), ion exchangers (Ulibarri & Hermosín, 2001), and additives (Leroux & Besse, 2004 – see also Rives, 2001, for a review). These compounds are also referred to as anionic clays or hydrotalcites, from the most common mineral species of this group. Their structure consists of a brucite-like octahedral layer in which some of the M^{2+} cations are replaced isomorphically by M^{3+}. The presence of interlayer anions compensates for the excess positive charge of the layer, whereas H_2O molecules may occupy the remaining interlayer space. As expandable layered silicates, LDHs have the ability to host a variety of interlayer anions and to exchange them dynamically. Similar to expandable layered silicates, the regular interstratification of layers hosting different interlayer anions is not common, but has been described even in naturally occurring varieties. For example, Drits *et al.* (1987) inferred the regular 1:1 interstratification of $Mg_{(3-x)}Al_x(OH)_6$ layers having CO_3^{2-} and SO_4^{2-} anions in their interlayers from the comparison of calculated XRD patterns with those recorded for samples from saline deposits. According to Iyi *et al.* (2007), LDH hydration as a function of RH is also reminiscent of expandable layered silicates: LDHs exhibit a stepwise increase of their layer-to-layer distance upon the incorporation of additional H_2O molecules. Those authors also reported the coexistence of different hydration states within the same crystals as shown by the presence of super-reflections corresponding to the regular alternation of dehydrated and hydrated interlayers. Super-reflections were observed in particular for their higher-charge LDH sample with two large interlayer anions (ClO_4^- and I^-). These observations are consistent with the early works of Brindley & Kikkawa (1980). Newman *et al.* (1998) and Iyi *et al.* (2002) described also the

regular interstratification of different hydration states and different interlayer configurations in Mg_2Al LDHs containing a single organic anion (terephtalate and azobenzene derivative, respectively).

Recently, intercalation of LDHs has attracted much interest because this process can modify their electronic, magnetic and optical properties by host-guest effect. Special efforts have been devoted to the simultaneous intercalation of LDHs with different guest species aiming at the synthesis of polyfunctional materials. Over the last decade or so, the development of energy-dispersive XRD on synchrotron sources has been especially useful to investigate the kinetics of intercalation (Fogg *et al.*, 1998a, 1998b; O'Hare *et al.*, 2000). In particular, this technique has allowed us to uncover the formation of 'intermediate' heterostructures corresponding to second staging, or regular 1:1 interstratification, of layers with different interlayer anions, similar to those described in amphiphilic modified clay structures (Ijdo *et al.*, 1996; Ijdo & Pinnavaia, 1998a, 1998b). Such heterostructures, as determined from the presence of a superreflection characteristic of the regular interstratification (1:1 ratio, $S = 1$ with MPDO), have been reported for a variety of octahedral layer compositions and interlayer anions (Fig. 17a – Fogg *et al.*, 1998a, 1998b; Kayenoshi & Jones, 1998; O'Hare *et al.*, 2000; Pisson *et al.*, 2003; Williams *et al.*, 2003, 2004; Taviot-Guého *et al.*, 2005, 2010; Williams & O'Hare, 2005, 2006; Feng *et al.*, 2006; Zhang *et al.*, 2008; Ragavan *et al.*, 2009). It should be noted that the regular distribution (second staging) of inorganic and organic interlayers can be maintained through subsequent exchange of one of the guest anions as shown by Williams & O'Hare (2006) for the adipate-for-succinate or the adipate-for-tartrate exchange in a Zn_2Cr LDH initially containing Cl^- in addition to the organic anion.

Beside these numerous reports of regularly interstratified mixed layers, additional kinetic studies of the anion-exchange process describe the steady migration of peaks from one end-member to the other during the anion-exchange process (Feng *et al.*, 2006; Taviot-Guého *et al.*, 2010; Fig. 17b), similar to the diffraction behaviour described by Méring for the random interstratification of different layer types (Méring, 1949). Significant variations in the position and breadth of the diffraction peak characteristic of the regular interstratification of two layer types has also been reported for the carbonate-for-tartrate exchange in a Zn_2Cr LDH (Feng, 2006; Fig. 17c). Such variation indicates that the alternation of carbonate and tartrate interlayers departs from the regular 1:1 alternation. Both a carbonate:tartrate ratio other than the 1:1 ratio and junction probabilities other than the $S = 1$ case with MPDO, *i.e.* partial ordering, can account for the observed variation. These non-regular mixed layers have received much less attention than their regular counterparts, however, and stacking sequences have not even been determined.

The alternation, regular or otherwise, of different layer types in LDHs will impact not only the position and profiles of 00*l* basal reflections as described above, but also the position and profiles of non-basal '*hkl*' lines as most LDHs possess a 3D periodicity. Bookin & Drits (1993) reported theoretical calculations performed for all possible LDH structure models, *i.e.* for all possible stacking modes (polytypic fragments) resulting from the different interlayer configurations. The positions and relative intensities

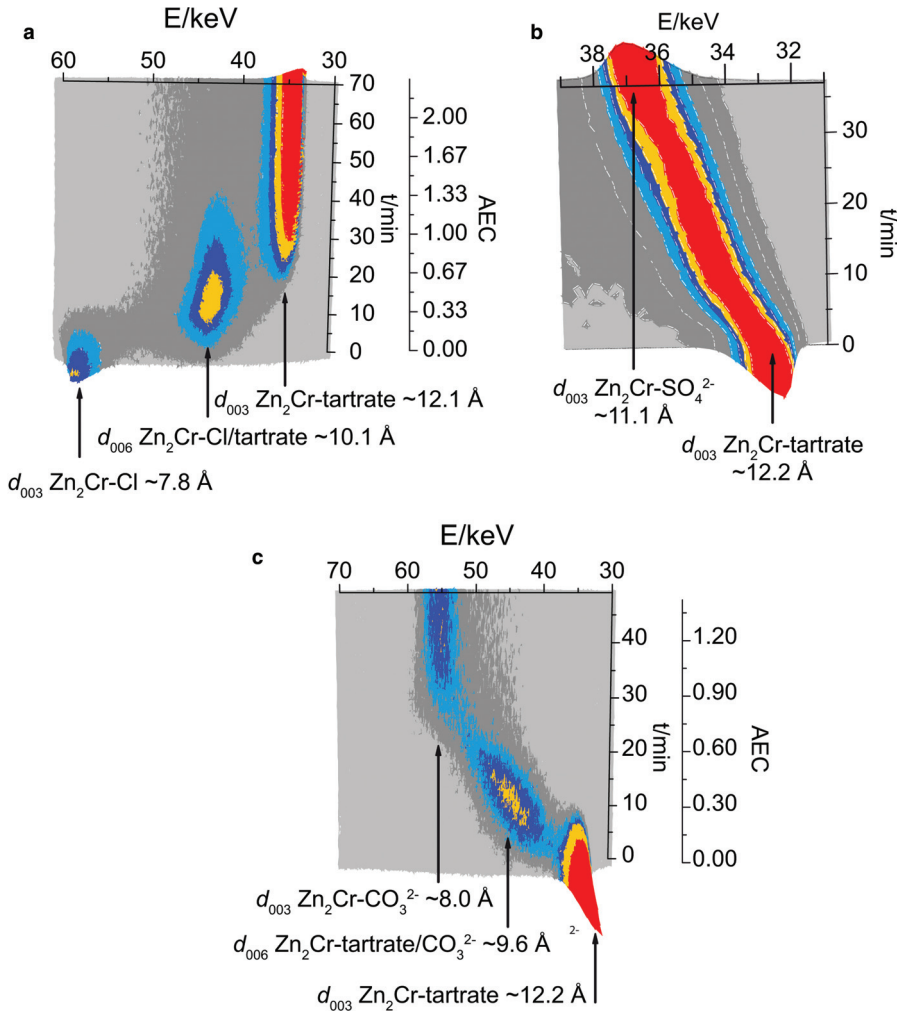

Fig. 17. Dynamic evolution of XRD patterns during the anion exchange of Zn_2Cr LDHs. (***a***) Tartrate-for-chlorine exchange, showing a super-periodicity corresponding to the regular alternation of the two anions in successive interlayers (2nd staging – adapted from Feng, 2006). (***b***) Sulphate-for-tartrate exchange, showing a steady shift of peak position from one end-member to the other, characteristic of the random interstratification of the two types of anions in successive interlayers (adapted from Taviot-Guého *et al.*, 2010). (***c***) Carbonate-for-tartrate exchange (adapted from Feng, 2006). Compared to Figure 17a the peak corresponding to the super-periodicity is shifting as the exchange proceeds, thus suggesting a carbonate:tartrate ratio different from 50:50 in a stacking which is predominantly ordered. For the Zn_2Cr LDH with interlayer tartrate, carbonate, sulphate and chlorine anions the d_{003} values correspond to the layer-to-layer distance because of the 3*R* polytype. For the Zn_2Cr LDH with mixed Cl^-/tartrate or tartrate/CO_3^{2-} anion composition, the d_{006} values correspond to the second order of the basal distance corresponding to the periodic repetition of the two anions in successive interlayers (2nd staging). The AEC scale indicates the amount of tartrate (***a***), SO_4^{2-} (***b***), or CO_3^{2-} (***c***) anions added in solution during these dynamic experiments expressed as a fraction of the anion exchange capacity.

reported for the different LDH polytypes can serve to determine the actual stacking mode, and polytypic variety, of periodic species (Bookin *et al.*, 1993), but can serve also as a basis for the interpretation of diffraction effects arising from the interstratification of different polytypic fragments (Drits & Bookin, 2001). A number of structural studies have actually investigated the interstratification of such structural fragments from the profiles of non-basal reflections, essentially using the recursive description of the layers' stacking and the *DIFFaX* code (Bellotto *et al.*, 1996; Thomas *et al.*, 2004; Radha *et al.*, 2005, 2010; Thomas & Kamath, 2006; Curtius & Ufer, 2007; Radha & Kamath, 2009). These studies consistently show the random interstratification of common rhomboedral, hexagonal, and eventually monoclinic LDH polytype fragments from the migration of the *hkl* reflections corresponding to the predominant polytype towards neighbouring reflections of the minor polytype, which is described as a well defined stacking fault.

3.4. Interstratification of other lamellar structures: layered oxides

3.4.1. Interstratification of commensurate polytype fragments

Interstratification of polytypic fragments has been reported also in layered oxides. For example, in the general context of preparation of heterostructured hybrid materials, Du & O'Hare (2008) reported second staging in α-Co hydroxides from the presence of super-reflections corresponding to the regular interstratification of two layer types. The regular alternation of DDS (dodecyl sulphate) and carbonate layers (27.8 and 8.2 Å, respectively) over extended length scales was confirmed from lattice-fringe images obtained under the TEM.

Interstratification of layers having different layer-to-layer distances has also been reported in $Ni(OH)_2$, which is the positive electrode material of nickel-based alkaline secondary batteries (Ni-Cd, Ni-metal hybride, Ni-H_2). Two main structures have been reported for this material. α-$Ni(OH)_2$ is a turbostratic phase exhibiting a basal distance of ∼8.4 Å, whereas β-$Ni(OH)_2$ corresponds to the 1*H* polytype and has a ∼4.6 Å unit-cell length perpendicular to the layer plane. Using a recursive description of stacking sequences, Ramesh *et al.* (2003) investigated systematically the impact of the random interstratification of these two polytypes on XRD patterns. The influence of such stacking faults on the position and profiles of basal 00*l* reflections was used to report not only their occurrence but also to assess their abundance (relative proportions of the two polytypes – Rajamathi *et al.*, 2000; Tessier *et al.*, 2000a; Ramesh *et al.*, 2003, 2005). The presence of stacking faults in β-$Ni(OH)_2$ not only modifies the position and profile of basal 00*l* reflections, but also impacts non-basal *hkl* reflections as shown for growth and deformation faults (Delmas & Tessier, 1997; Tessier *et al.*, 1999). Within the 1*H* stacking sequences of β-$Ni(OH)_2$ (AbC AbC AbC . . .), these two types of faults correspond to the occurrence of twinning (AbC AbC CbA CbA . . .) and to a $-a/3$ layer displacement (AbC AbC CaB CaB . . .) and induce a significant broadening of 101 and 102 lines compared to other reflections. Tessier *et al.* (1999), Ramesh *et al.* (2003), and Ramesh (2009) calculated systematically the influence of different stacking faults on β-$Ni(OH)_2$ XRD patterns. These calculations were subsequently used to describe,

from the modelling of XRD data, the occurrence and abundance of a variety of stacking faults in β-$Ni(OH)_2$ (Delmas & Tessier, 1997; Tessier *et al.*, 1999, 2000a; Guerlou Demourgues *et al.*, 2004; Ramesh *et al.*, 2005, 2006; Ramesh & Kamath, 2008a; Ramesh, 2009). Other structural parameters such as the size of the CSDs and the abundance of vacant layer sites or of isomorphous cationic substitutions, for example, were also determined in some of these studies (Ramesh *et al.*, 2003, 2005, 2006; Ramesh, 2009). In an elegant paper, Ramesh & Kamath (2008b) demonstrated that the quality of the structural characterization is improved significantly, compared to a 'usual' Rietveld refinement, when stacking faults are characterized and quantified, even if the abundance of these faults is limited to a few percent. Finally, clear correlations were determined between the nature and abundance of some of the above defects and the synthesis conditions (Tessier *et al.*, 2000a, 2000b; Guerlou Demourgues *et al.*, 2004; Ramesh *et al.*, 2006) or electrochemical properties of these materials, such as chargeability and electronic conductivity (Tessier *et al.*, 1999; Ramesh & Kamath, 2008a; Ramesh, 2009).

Layered MnO_2 (birnessite or δ-MnO_2) has attracted a sustained interest over the last two decades owing to its ubiquity in superficial oxic environments where its ability to degrade organic pollutants and to fix trace-metal elements has a pivotal influence on the fate of these contaminants, in addition to its potential as a cathode material. As for $Ni(OH)_2$, different stacking sequences have been reported for birnessite octahedral layers, that can also have different symmetry depending on the origin of the layer-charge deficit. Layers with hexagonal symmetry, and small *b* unit-cell dimensions (2.84–2.85 Å), are characterized by small amounts of Mn^{3+} cations within the octahedral layer, with large layer-vacancy contents being responsible for the layer-charge deficit. On the contrary, when layers are almost devoid of vacancies, the layer-charge deficit arises essentially from the presence of layer Mn^{3+} cations (25–30%). In this case, Jahn-Teller distorted Mn^{3+} octahedra are ordered at room temperature to minimize the steric strains, and their systematic elongation along the *a* axis leads to an orthogonal layer symmetry with $a > b \times \sqrt{3}$ (Gaillot *et al.*, 2007). Drits *et al.* (2007a) calculated systematically the intensity distribution for all possible polytypes, and relevant associated interlayer configurations, thus providing a sound basis for the identification of these polytypes, but also for the prediction of the diffraction effects arising from their random interstratification. These authors also described the layer symmetry and stacking sequences for most varieties reported in the literature at that time as a function of the synthesis conditions. Owing to this polytypic diversity, 3D-ordered birnessite varieties often appear as mixed layers in which different polytypic fragments are interstratified, as in $Ni(OH)_2$. For example, interstratification of the 1*H* polytype, which is the stable form of birnessite when equilibrated at low pH, with other polytypic variants has been described (Manceau *et al.*, 1997; Lanson *et al.*, 2000, 2002b). By taking into account the interstratification of the different polytypes, it was possible to extract additional structural information from the XRD patterns of these defective structures (Fig. 18). In particular, the number of vacant octahedral sites, the number, location and coordination of interlayer transition metal cations, and the number and location of interlayer H_2O molecules were determined systematically. Interpretation of these fine structure

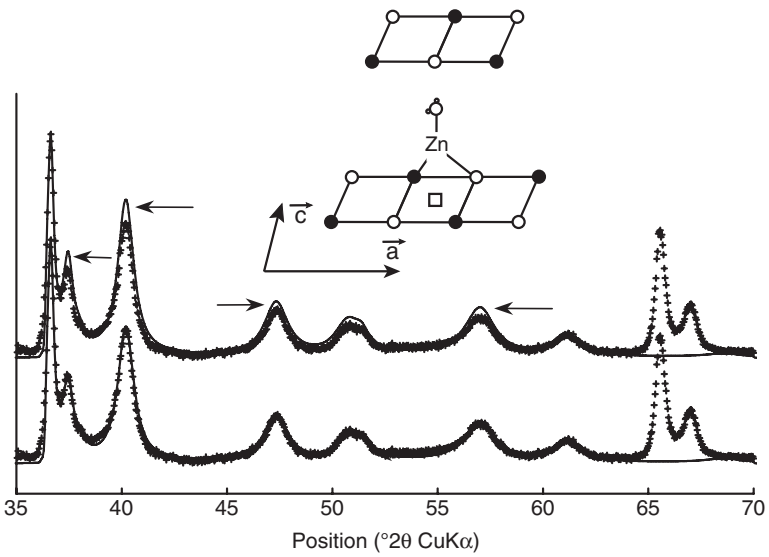

Fig. 18. Comparison between experimental and calculated diffraction patterns for the phyllomanganate birnessite equilibrated at low pH in the presence of Zn (adapted from Lanson *et al.*, 2002b). The agreement between calculated and experimental intensity distributions is significantly improved when both tetrahedral and octahedral coordinations are considered for interlayer Zn cations (0.078:0.040 ratio – bottom) as compared to a unique octahedral coordination (top). The tetrahedral coordination of Zn located above, or below, vacant octahedral layer sites provides additional bonding between adjacent layers shifted by $+a/3$, through the formation of strong H-bonds. Symbols as in Figure 5.

details allowed us to unravel the H-bonding responsible for the respective stability of the different stacking modes (Lanson *et al.*, 2000, 2002b), but also the reaction mechanisms involved in the high to low pH structural transition occurring in birnessite (Lanson *et al.*, 2000) or those leading to the oxidation of Co^{2+} and to its incorporation in the MnO_2 octahedral layer (Manceau *et al.*, 1997). The different polytypes resulting from contrasting synthesis conditions most often include minor amounts of other polytypic fragments randomly interstratified within the main stacking sequence (Gaillot *et al.*, 2003, 2004, 2005). For example, Gaillot *et al.* (2003) were able to refine the structure of a specific 2*H* polytype from a μm-sized monocrystal, but had to consider the contribution from a 2*H*/3*R* mixed layer to fit the powder XRD pattern recorded for the whole sample. Drits *et al.* (1998a) even reported the complex interstratification of two 4-layer polytypes, in addition to the presence of one of these polytype as a 3D-periodic species. Finally, interstratification of layers having the same stacking vector within the *ab* plane but differing in their layer-to-layer distance was described during the dehydration of birnessite at moderate (100–150°C) temperature (Gaillot *et al.*, 2005).

3.4.2. Interstratification of incommensurate fragments

Interstratification may occur between layers each having their own 2D periodicity and irrational *a* and/or *b* unit-cell parameters (Drits, 1987, 2003; Organova, 1989;

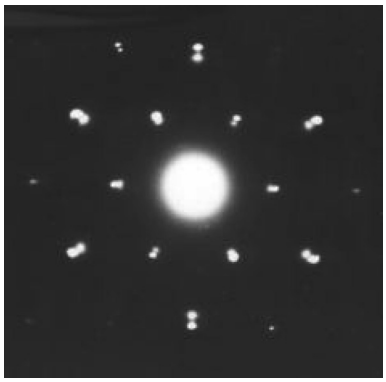

Fig. 19. Electron diffraction pattern from a Co-asbolane exhibiting reflection networks corresponding to the two incommensurate layers (from Gaillot, 2002).

Makovicky & Hyde, 1992). As a result, the individual structures of these layers can be described with two independent unit cells, and selected area electron diffraction is an especially powerful tool to unravel the interstratification of such incommensurate layers (Fig. 19). For example, the regular alternation, along the axis perpendicular to the layer plane, of octahedral layers having different compositions defines a peculiar group of phyllomanganates whose natural occurrences are reported under the generic name of asbolane (Chukhrov *et al.*, 1982, 1989; Drits, 1985; Manceau *et al.*, 1992; Feng *et al.*, 2001). In these peculiar mixed layers, the MnO_2 layer is continuous whereas the other layer type essentially forms island-like domains sandwiched between the MnO_2 layers to allow for the formation of H-bonds that ensure the overall stacking stability. Regular alternation of incommensurate layers has also been described for other compositions. For example, alternation of brucite and sulphide layers was reported in the minerals valleriite and tochilinite (Evans & Allman, 1968; Organova *et al.*, 1974; Drits, 1987; Organova, 1989). The natural occurrence of regularly alternating chrysotile and hydrotalcite layers was also reported (Drits *et al.*, 1995).

Using the theoretical developments of Plançon (1981), Gaillot *et al.* (2004) revealed a new type of structural disorder in layered structures with the random alternation of partially incommensurate layers. These authors reported the interstratification of layers having hexagonal and orthogonal symmetry, but the same basal distance and the same stacking vectors. In this case, *hk* rods corresponding to the interstratified layer types overlap partially, giving rise to very specific diffraction features. In particular, the breadth of *hkl* reflections corresponding to the mixed layer decreases with increasing values of the Miller index *l*.

3.5. Structural characterization of disordered layered structures

As described in section 2.1.2., the occurrence of random stacking faults leads to diffraction effects strikingly different from those described above. In particular, the resolution of *hkl* reflections is progressively lost when increasing the proportion of such random stacking faults (Fig. 2). In turbostratic compounds, random stacking faults occur systematically between adjacent layers thus inducing 2D crystals, characterized by an asymmetric diffraction profile (*hk* diffraction band) similar to that obtained from a single layer, in addition to 00*l* reflections.

Warren (1941) soon recognized that it was possible to decipher structural information from the profile of *hk* bands, despite the absence of resolved *hkl* lines (Biscoe & Warren, 1942). In their pioneering work, Warren (1941) and Biscoe & Warren (1942) were able, from the analysis of XRD data, to prove the 2D periodicity of carbon blacks and to

determine their CSD size within the layer plane. Further information on the actual 2D structure of layers can be retrieved from the modelling of *hk* band profiles. These bands are similar to the structure factor of a single layer and thus comprise the coordinates and occupancies for all atomic sites within the layer. Leoni (2008) reviewed existing methods used to retrieve structural information from such diffraction patterns. The next section will deal with recent results obtained with these different approaches.

3.5.1. Layered silicates

Despite recent studies that challenged the actual turbostratic character of expandable layered silicates (Viani *et al.*, 2002), *hk* band profiles of smectite have been used widely to investigate the 3D organization of their interlayer cations and H_2O molecules (Brindley & Méring, 1951; Méring & Brindley, 1967). Ben Brahim *et al.* (1984) used a similar approach to investigate the positions of cations and H_2O molecules in Na-beidellite, but had to describe also the layer stacking of their sample that was not totally turbostratic. In two articles devoted to the structural characterization of oxidized and reduced nontronite (Fe-rich smectite), Manceau *et al.* (2000a, 2000b) modelled the profiles and relative intensities of the 02,11 and 20,13 bands, to determine the actual occupancy of the different octahedral sites, and in particular, to assess the presence of cations occupying *trans* sites in the essentially *trans*-vacant oxidized species. They showed that all nontronite samples investigated were 100% *trans*-vacant, with a detection limit of $\sim$10% for occupied *trans*-sites. In the companion article devoted to the structural characterization of reduced nontronites (Manceau *et al.*, 2000a), these authors showed the formation of trioctahedral clusters induced by the migration of reduced Fe cations within the octahedral sheet of the smectite layer. Trioctahedral clusters induce in particular a modification of the intensity distribution between 02,11 and 20,13 bands as predicted by Drits *et al.* (1984). They also showed the induced reduction of the CSD size, and the lowering of the original hexagonal layer symmetry hexagonal to an orthogonal one ($b > a \times \sqrt{3}$). The analysis of *hk* band profiles, and especially of their relative intensities, even allowed the presence of Fe cations with tetrahedral coordination within smectite layers to be unravelled and quantified when the Fe content was sufficient (Manceau *et al.*, 2000b; Gates *et al.*, 2002).

3.5.2. Layered oxides

In natural environments, disordered varieties of phyllomanganates (birnessite and its disordered analogue vernadite, or δ-MnO_2) prevail probably as a result of the biogenically mediated oxidation of Mn^{2+}. Modelling studies, similar to those performed on layered silicates, have been carried out recently to determine their layer structure, and, in particular, the origin of the layer-charge deficit (presence of Mn^{3+} cations or of vacant sites within the octahedral layer), and to assess the induced density of reactive sites. From theoretical calculations, Drits *et al.* (2007a) reported the influence of these parameters, but also of the number, location, nature, and coordination of interlayer species on the profile of *hk* bands. In a few reports, the splitting of *hk* bands can be interpreted qualitatively to prove the orthogonal symmetry of the layer, and thus the

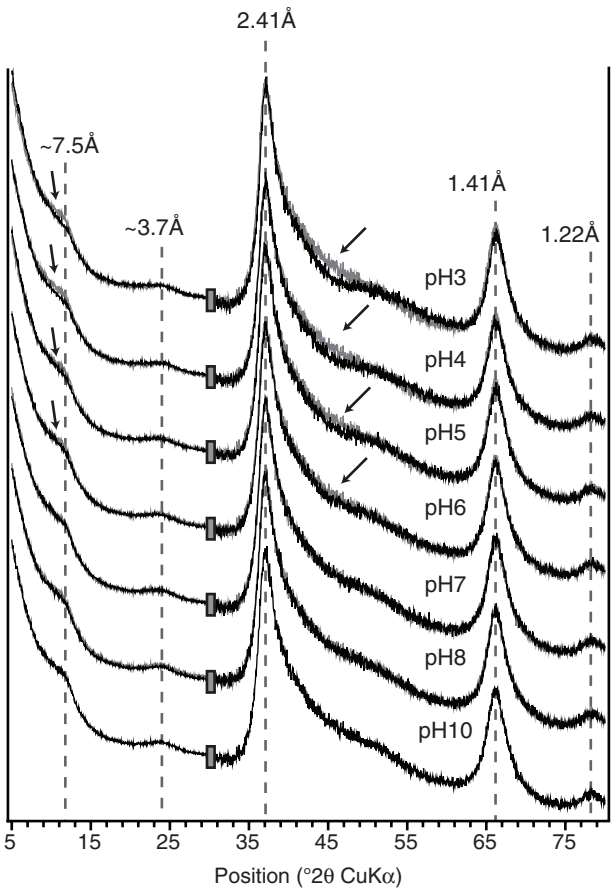

Fig. 20. XRD patterns recorded for the phyllomanganate vernadite (turbostratic birnessite variety) when equilibrated at different pH values (adapted from Grangeon, 2008). The XRD pattern recorded on the pH10 sample is shown systematically as a grey trace to emphasize the differences in the profile shape of the *hk* band at 2.41 Å (arrows). The observed profile modification is linked to the steadily increasing number of interlayer Mn cations located above vacant layer sites when decreasing the pH from 10 (0.075 interlayer Mn cation per layer octahedron) to 3 (0.175 interlayer Mn cation per layer octahedron).

prevailing influence of Mn^{3+} cations within the octahedral sheet (Webb *et al.*, 2005; Zhu *et al.*, 2010). Most often, the layer symmetry is hexagonal, thus indicating the predominant contribution of vacant layer sites to the layer-charge deficit (Fig. 20) (Jurgensen *et al.*, 2004; Villalobos *et al.*, 2006; Grangeon *et al.*, 2008, 2010; Lanson *et al.*, 2008). Depending on the synthesis protocol, or on the living organism responsible for Mn^{2+} oxidation, differences in the profile shape of the decreasing high-angle tail of the 02,11 band reveal a significant scatter in the density of vacant layer sites and thus in the number of reactive sites for the adsorption of di- and trivalent transition metal cations (Villalobos *et al.*, 2006; Grangeon *et al.*, 2008, 2010; Lanson *et al.*, 2008). The size of CSDs, which is also a key factor in the reactivity of these materials from the influence on the relative contribution of edge sites, is also highly variable as a function of the conditions of formation. Finally, the location and coordination of interlayer species was determined, thus allowing a complete structural characterization of these compounds despite their intrinsic defective character. It should be noted that XRD patterns obtained for some of these compounds are actually devoid of 00*l* reflections, despite their undisputable lamellar character, because of the extreme delamination, these lamellar

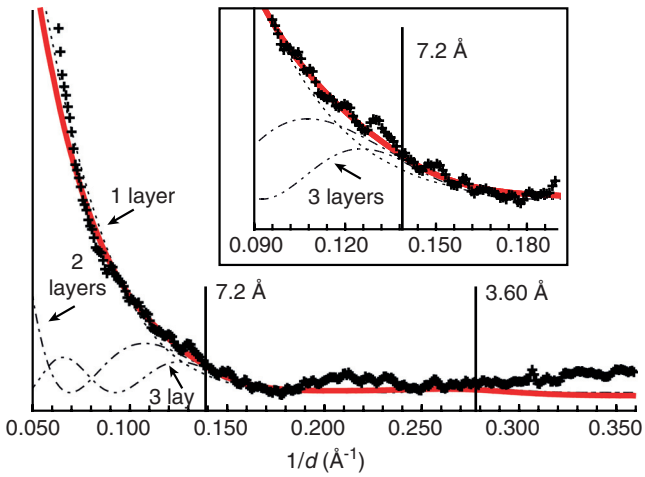

Fig. 21. Comparison between experimental and calculated diffraction patterns (00*l* basal reflections only) for the phyllomanganate vernadite formed in the roots of *Festuca rubra* (adapted from Lanson *et al.*, 2008). 001 and 002 reflections are calculated for crystallites composed of one (dashed line), two (dotted-dashed line) and three (dot-dot-dashed line) parallel layers. The optimal fit (red line) to the data (crosses) is obtained with an assemblage of diffracting crystallites containing 1, 2, and 3 layers in the ratio of 2.0:0.3:0.1. Readers of the paper version of this chapter may wish to download a colour version of this figure from www.minersoc.org/emu-notes/emu-11/11-4-colour.pdf.

compounds occurring essentially as single layers bound together by organic matter (Fig. 21 – Lanson *et al.*, 2008; Grangeon *et al.*, 2010).

4. Conclusions

Modelling of XRD data has been used increasingly over the last few decades to determine the nature, abundance and distribution of structure defects in lamellar compounds. For example, structure models were determined for 2D periodic species that are commonly described as amorphous owing to the absence of resolved *hkl* reflections. Similarly, the nature, abundance and distribution of well defined stacking faults have been uncovered in 3D ordered structures, and the nature of interstratified layer types and their stacking sequences were characterized. Owing to the increased potential of calculation routines, such studies could be carried out successfully even on polyphasic and/or natural samples. In all cases, they provided additional understanding of these complex structures, and the structural parameters determined often proved to be key factors for the comprehension of the material/mineral reactivity. Structural parameters such as layer-stacking sequences in mixed layers were also essential to determine their reaction mechanisms, and, ultimately, to determine thermodynamic data relevant to these systems and possibly the kinetic effects affecting these reactions. As the number of parameters required to describe completely defective structures is increased compared to

common structure refinements, additional constraints, either experimental or computational, are extremely beneficial to support proposed structure models. In turn, taking into account structure defects and heterogeneity affecting layered compounds allows us to match more accurately the complementary data. The need to use such a large number of complementary techniques (microscopies, spectroscopies, chemical and thermal analyses, ...) in order to constrain or complement XRD structural studies is emphasized as it is often essential in order to obtain an unambiguous and comprehensive structure model (Drits, 1983, 2003; McCarty *et al.*, 2004; Lindgreen *et al.*, 2008; Drits *et al.*, 2010).

The modelling approach represents the optimum, and at present the sole, quantitative method allowing a thorough structure determination of defective lamellar compounds. This approach has allowed us to reveal the intrinsic complexity of defective lamellar structures and to improve their structural characterization. Lanson *et al.* (2002a) and Ramesh & Kamath (2008b) showed, for example, that structural characterization is significantly enhanced when stacking faults are characterized and quantified, even if the abundance of these faults is limited to a few percent. In addition, the modelling approach has allowed us to unravel specific properties of elementary layers, such as fluctuations of the layer-to-layer distance, or to refine their actual structure. The ability to calculate diffraction effects from multi-component mixed layers has also allowed us to reveal their ubiquitous presence in both natural and synthetic samples, and the frequent contribution to the diffraction intensity of mixed layers lacking a characteristic diffraction fingerprint in the low-angle region. The calculation routines available have refreshed the description of defective structures and a key point when using these tools is thus 'imagination': the search for possible structure models should not be restricted to those that have already been reported in the literature. A wider application of these tools to natural and synthetic samples will undoubtedly allow for new fundamental findings.

The use of these methods remains restricted, however, essentially because of the limited coupling between defective-structure calculation routines and automatic minimization ones. However, when sought, this coupling should not be detrimental to the versatility of the calculation routines. A trial-and-error optimization of the structure model will undoubtedly slow down the characterization, or hamper its generalization to large sample sets, but an (over-)simplified calculation routine will just preclude it. When comprehensive modelling is not performed, direct comparison between experimental XRD patterns and those calculated from the hypothesized structure remains crucial to assess the validity, and possibly the limits, of the proposed structure model.

References

Allegra, G. (1961) A simplified formula for the calculation of the X-ray intensity diffracted by a monodimensionally disordered structure. *Acta Crystallographica*, **14**, 535.

Allegra, G. (1964) The calculation of the intensity of X-rays diffracted by monodimensionally disordered structures. *Acta Crystallographica*, **14**, 579–586.

Aplin, A.C., Matenaar, I.F., McCarty, D.K. & van Der Pluijm, B.A. (2006) Influence of mechanical compaction and clay mineral diagenesis on the microfabric and pore-scale properties of deep-water Gulf of Mexico Mudstones. *Clays and Clay Minerals*, **54**, 500–514.

Argüelles, A., Leoni, M., Blanco, J.A. & Marcos, C. (2010) Semi-ordered crystalline structure of the Santa Olalla vermiculite inferred from X-ray powder diffraction. *American Mineralogist*, **95**, 126–134.

Bailey, S.W., Brindley, G.W., Kodama, H. & Martin, R.T. (1982) Report of the Clay Minerals Society Nomenclature Committee for 1980–1981: Nomenclature for regular interstratifications. *Clays and Clay Minerals*, **30**, 76–78.

Beaufort, D., Baronnet, A., Lanson, B. & Meunier, A. (1997) Corrensite: A single phase or a mixed-layer phyllosilicate in the saponite-to-chlorite conversion series? A case study of Sancerre-Couy deep drill hole (France). *American Mineralogist*, **82**, 109–124.

Bellotto, M., Rebours, B., Clause, O., Lynch, J., Bazin, D. & Elkaïm, E. (1996) A reexamination of hydrotalcite crystal chemistry. *Journal of Physical Chemistry*, **100**, 8527–8534.

Ben Brahim, J., Armagan, G., Besson, G. & Tchoubar, C. (1983) X-ray diffraction studies on the arrangement of water molecules in a smectite. I. Homogeneous two-water-layer Na-beidellite. *Journal of Applied Crystallography*, **16**, 264–269.

Ben Brahim, J., Besson, G. & Tchoubar, C. (1984) Etude des profils des bandes de diffraction X d'une beidellite-Na hydratée à deux couches d'eau. Détermination du mode d'empilement des feuillets et des sites occupés par l'eau. *Journal of Applied Crystallography*, **17**, 179–188.

Bérend, I., Cases, J.M., François, M., Uriot, J.P., Michot, L.J., Masion, A. & Thomas, F. (1995) Mechanism of adsorption and desorption of water vapour by homoionic montmorillonites: 2. The Li^+, Na^+, K^+, Rb^+ and Cs^+ exchanged forms. *Clays and Clay Minerals*, **43**, 324–336.

Bergmann, J. & Kleeberg, R. (1998) Rietveld analysis of disordered layer silicates. In: *Proceedings of the European Powder Diffraction (EPDIC5)* (R. Delhez & E.J. Mittemeijer, editors), p. 300–305.

Besson, G., Glaeser, R. & Tchoubar, C. (1983) Le césium, révélateur de structure des smectites. *Clay Minerals*, **18**, 11–19.

Bethke, C.G., Vergo, N. & Altaner, S.P. (1986) Pathways of smectite illitization. *Clays and Clay Minerals*, **34**, 125–135.

Biscoe, J. & Warren, B.E. (1942) An X-ray study of carbon black. *Journal of Applied Physics*, **13**, 364–371.

Bookin, A.S. & Drits, V.A. (1993) Polytype diversity of the hydrotalcite-like minerals. I. Possible polytypes and their diffraction features. *Clays and Clay Minerals*, **41**, 551–557.

Bookin, A.S., Drits, V.A., Plançon, A. & Tchoubar, C. (1989) Stacking faults in kaolin-group minerals in the light of real structural features. *Clays and Clay Minerals*, **37**, 297–307.

Bookin, A.S., Cherkashin, V.I. & Drits, V.A. (1993) Polytype diversity of the hydrotalcite-like minerals. II. Determination of the polytypes of experimentally studied varieties. *Clays and Clay Minerals*, **41**, 558–564.

Breu, J., Seidl, W., Stoll, A.J., Lange, K.G. & Probst, T.U. (2001) Charge homogeneity in synthetic fluorohectorite. *Chemistry of Materials*, **13**, 4213–4220.

Brindley, G.W. & Kikkawa, S. (1980) Thermal behavior of hydrotalcite and of anion-exchanged forms of hydrotalcite. *Clays and Clay Minerals*, **28**, 87–91.

Brindley, G.W. & Méring, J. (1951) Diffraction des Rayons X par les Structures en Couches Désordonnées. *Acta Crystallographica*, **4**, 441–447.

Brindley, G.W., Suzuki, T. & Thiry, M. (1983) Interstratified kaolinite/smectites from the Paris Basin; Correlations of layer proportions, chemical compositions and other data. *Bulletin de Minéralogie*, **106**, 403–410.

Calarge, L., Lanson, B., Meunier, A. & Formoso, M.L. (2003) The smectitic minerals in a bentonite deposit from Melo (Uruguay). *Clay Minerals*, **38**, 25–34.

Cases, J.M., Bérend, I., François, M., Uriot, J.P., Michot, L.J. & Thomas, F. (1997) Mechanism of adsorption and desorption of water vapour by homoionic montmorillonite: 3. the Mg^{2+}, Ca^{2+}, Sr^{2+} and Ba^{2+} exchanged forms. *Clays and Clay Minerals*, **45**, 8–22.

Cavani, F., Trifirò, F. & Vaccari, A. (1991) Hydrotalcite-type anionic clays: Preparation, properties and applications. *Catalysis Today*, **11**, 173–301.

Cesari, M. & Allegra, G. (1967) The intensity of X-rays diffracted by monodimensionally disordered structures: Case of identical layers and three different translation vectors. *Acta Crystallographica*, **23**, 200–205.

Cesari, M., Morelli, G.L. & Favretto, L. (1965) The determination of the type of stacking in mixed-layer clay minerals. *Acta Crystallographica*, **18**, 189–196.

Chipera, S.J. & Bish, D.L. (2001) Baseline studies of the Clay Minerals Society Source Clays: Powder X-ray diffraction analyses. *Clays and Clay Minerals*, **49**, 398–409.

Chukhrov, F.V., Gorshkov, A.I., Vitovskaya, I.V., Drits, V.A., Sistov, A.V. & Rudnitskaya, Y.S. (1982) Crystallochemical nature of Co-Ni asbolane. *International Geology Review*, **24**, 598–604.

Chukhrov, F.V., Gorshkov, A.I. & Drits, V.A. (1989) *Supergenic manganese hydrous oxides*. Nauka, Moscow, 208 pp.

Claret, F., Sakharov, B.A., Drits, V.A., Velde, B., Meunier, A., Griffault, L. & Lanson, B. (2004) Clay minerals in the Meuse-Haute marne underground laboratory (France): Possible influence of organic matter on clay mineral evolution. *Clays and Clay Minerals*, **52**, 515–532.

Cuadros, J. (2002) Structural insights from the study of Cs-exchanged smectites submitted to wetting-and-drying cycles. *Clay Minerals*, **37**, 473–486.

Curtius, H. & Ufer, K. (2007) Eu incorporation behavior of a Mg-Al-Cl layered double hydroxide. *Clays and Clay Minerals*, **55**, 354–360.

Cygan, R.T., Liang, J.-J. & Kalinichev, A.G. (2004) Molecular models of hydroxide, oxyhydroxide, and clay phases and the development of a general force field. *Journal of Physical Chemistry B*, **108**, 1255–1266.

D'yakonov, Y.S. (1961) Application of Fourier transform methods for the interpretation of mixed-layer mineral diffraction patterns. *Kristallografia*, **6**, 624–625 (in Russian).

D'yakonov, Y.S. (1962) Interpretation of mixed-layer mineral diffraction patterns by direct methods of Fourier transforms (in Russian). In: *X-ray Study of Mineral Raw Materials* (G.A. Sidorenko, editor). Nedra, Moscow, pp. 34–42.

de la Calle, C., Pezerat, H. & Gasperin, M. (1977) Problèmes d'ordre-désordre dans les vermiculites: Structure du minéral calcique hydraté à deux couches. *Journal de Physique*, **C7**, 128–133.

de la Calle, C., Suquet, H. & Pons, C.H. (1988) Stacking order in a 14.30 Å Mg-vermiculite. *Clays and Clay Minerals*, **38**, 481–490.

Delmas, C. & Tessier, C. (1997) Stacking faults in the structure of nickel hydroxide: a rationale of its high electrochemical activity. *Journal of Materials Chemistry*, **7**, 1439–1443.

Drits, V.A. (1983) Some aspects of the study of the real crystal structure of clay minerals. In: *Proceedings of the 5th Meeting of the European Clay Groups (Prague)* (J. Konta, editor), Univerzita Karlova, Prague, pp. 33–42.

Drits, V.A. (1985) Mixed-layer minerals: Diffraction methods and structural features. In: *Proceedings of the International Clay Conference (Denver)* (L.G. Schultz, H. Van Olphen & F.A. Mumpton, editors). The Clay Minerals Society, Boulder, Colorado, USA, pp. 33–45.

Drits, V.A. (1987) *Electron Diffraction and High-resolution Electron Microscopy of Mineral Structures*. Springer Verlag, Berlin, Heidelberg, 304 pp.

Drits, V.A. (1997) Mixed-layer minerals. In: *Modular Aspects of Minerals* (S. Merlino, editor). EMU Notes in Mineralogy, **1**, Eötvös University Press, Budapest, pp. 153–190.

Drits, V.A. (2003) Structural and chemical heterogeneity of layer silicates and clay minerals. *Clay Minerals*, **38**, 403–432.

Drits, V.A. & Bookin, A.S. (2001) Crystal structure and X-ray identification of layered double hydroxides. In: *Layered Double Hydroxides: Present and Future* (V. Rives, editor). Nova Science Publishers, New York, pp. 41–100.

Drits, V.A. & McCarty, D.K. (1996) The nature of diffraction effects from illite and illite-smectite consisting of interstratified *trans*-vacant and *cis*-vacant 2:1 layers: A semi-quantitative technique for determination of layer-type content. *American Mineralogist*, **81**, 852–863.

Drits, V.A. & Plançon, A. (1994) Expert system for structural characterization of phyllosilicates. II. Application to mixed-layer minerals. *Clay Minerals*, **29**, 39–45.

Drits, V.A. & Sakharov, B.A. (1976) *X-ray Structure Analysis of Mixed-layer Minerals*. Nauka, Moscow, 256 pp.

Drits, V.A. & Sakharov, B.A. (2004) Potential problems in the interpretation of powder X-ray diffraction patterns from fine-dispersed $2M_1$ and $3T$ dioctahedral micas. *European Journal of Mineralogy*, **16**, 99–110.

Drits, V.A. & Tchoubar, C. (1990) *X-ray Diffraction by Disordered Lamellar Structures: Theory and Applications to Microdivided Silicates and Carbons*. Springer-Verlag, Berlin, 371 pp.

Drits, V.A. & Zviagina, B.B. (2009) *Trans*-vacant and *cis*-vacant 2:1 layer silicates: Structural features, identification, and occurrence. *Clays and Clay Minerals*, **57**, 405–415.

Drits, V.A., Plançon, A., Sakharov, B.A., Besson, G., Tsipursky, S.J. & Tchoubar, C. (1984) Diffraction effects calculated for structural models of K-saturated montmorillonite containing different types of defects. *Clay Minerals*, **19**, 541–561.

Drits, V.A., Sokolova, T.N., Sokolova, G.V. & Cherkashin, V.I. (1987) New members of the hydrotalcite-manasseite group. *Clays and Clay Minerals*, **35**, 401–417.

Drits, V.A., Varaxina, T.V., Sakharov, B.A. & Plançon, A. (1994) A simple technique for identification of one-dimensional powder X-ray diffraction patterns for mixed-layer illite-smectites and other interstratified minerals. *Clays and Clay Minerals*, **42**, 382–390.

Drits, V.A., Gorshkov, A.I., Mokhov, A.V. & Pokrovskaya, E.V. (1995) New variety of mixed-layer mineral having unusual structure and morphology of crystals. *Lithology and Raw Materials*, **30**, 227–235 (in Russian).

Drits, V.A., Sakharov, B.A., Lindgreen, H. & Salyn, A. (1997) Sequential structure transformation of illite-smectite-vermiculite during diagenesis of Upper Jurassic shales from the North Sea and Denmark. *Clay Minerals*, **32**, 351–371.

Drits, V.A., Lanson, B., Gorshkov, A.I. & Manceau, A. (1998a) Substructure and superstructure of four-layer Ca-exchanged birnessite. *American Mineralogist*, **83**, 97–118.

Drits, V.A., Lindgreen, H., Salyn, A.L., Ylagan, R.F. & McCarty, D.K. (1998b) Semiquantitative determination of trans-vacant and cis-vacant 2:1 layers in illites and illite-smectites by thermal analysis and X-ray diffraction. *American Mineralogist*, **83**, 1188–1198.

Drits, V.A., Ivanovskaya, T.A., Sakharov, B.A., Gor'kova, N.V., Karpova, G.V. & Pokrovskaya, E.V. (2001) Pseudomorphous replacement of globular glauconite by mixed-layer chlorite-berthierine in the outer contact of dike: Evidence from the Lower Riphean Ust'Il'ya Formation, Anabar uplift. *Lithology and Mineral Resources*, **36**, 337–352.

Drits, V.A., Lindgreen, H., Sakharov, B.A., Jakobsen, H.J., Salyn, A.L. & Dainyak, L.G. (2002a) Tobelitization of smectite during oil generation in oil-source shales. Application to North Sea illite-tobelite-smectite-vermiculite. *Clays and Clay Minerals*, **50**, 82–98.

Drits, V.A., Sakharov, B.A., Dainyak, L.G., Salyn, A.L. & Lindgreen, H. (2002b) Structural and chemical heterogeneity of illite-smectites from Upper Jurassic mudstones of East Greenland related to volcanic and weathered parent rocks. *American Mineralogist*, **87**, 1590–1606.

Drits, V.A., Lindgreen, H., Sakharov, B.A., Jakobsen, H.J. & Zviagina, B.B. (2004) The detailed structure and origin of clay minerals at the cretaceous/tertiary boundary, Stevns Klint (Denmark). *Clay Minerals*, **39**, 367–390.

Drits, V.A., Sakharov, B.A., Salyn, A.L. & Lindgreen, H. (2005) Determination of the content and distribution of fixed ammonium in illite-smectite using a modified X-ray diffraction technique: Application to oil source rocks of western Greenland. *American Mineralogist*, **90**, 71–84.

Drits, V.A., Lanson, B. & Gaillot, A.C. (2007a) Birnessite polytype systematics and identification by powder X-ray diffraction. *American Mineralogist*, **92**, 771–788.

Drits, V.A., Lindgreen, H., Sakharov, B.A., Jakobsen, H.J., Fallick, A.E., Salyn, A.L., Dainyak, L.G., Zviagina, B.B. & Barfod, D.N. (2007b) Formation and transformation of mixed-layer minerals by tertiary intrusives in cretaceous mudstones, west Greenland. *Clays and Clay Minerals*, **55**, 260–283.

Drits, V.A., Ivanovskaya, T.A., Sakharov, B.A., Zvyagina, B.B., Derkowski, A., Gor'kova, N.V., Pokrovskaya, E.V., Savichev, A.T. & Zaitseva, T.S. (2010) Nature of the structural and crystal-chemical heterogeneity of the Mg-rich glauconite (Riphean, Anabar uplift). *Lithology and Mineral Resources*, **45**, 555–576.

Drits, V.A., Derkowski, A. & McCarty, D.K. (2011) New insight into the structural transformation of partially dehydroxylated pyrophyllite. *American Mineralogist*, **96**, 153–171.

Du, Y. & O'Hare, D. (2008) Observation of staging during intercalation in layered α-cobalt hydroxides: A synthetic and kinetic study. *Inorganic Chemistry*, **47**, 11839–11846.

Emmerich, K., Wolters, F., Kahr, G. & Lagaly, G. (2009) Clay profiling: The classification of montmorillonites. *Clays and Clay Minerals*, **57**, 104–114.

Evans, H.T. & Allman, R. (1968) The crystal structure and crystal chemistry of valleriite. *Zeitschrift für Kristallographie*, **127**, 73–93.

Feng, Q., Xu, Y.H., Kajiyoshi, K. & Yanagisawa, K. (2001) Hydrothermal soft chemical synthesis of Ni(OH)(2)-birnessite sandwich layered compound and layered LiNi1/3Mn2/3O2. *Chemistry Letters*, **30**, 1036–1037.

Feng, Y. (2006) *Formation and properties of second-stage layered double hydroxide materials*. PhD thesis, University of Clermont-Ferrand, France, 137 pp.

Feng, Y., Williams, G.R., Leroux, F., Taviot-Guého, C. & O'Hare, D. (2006) Selective anion-exchange properties of second-stage layered double hydroxide heterostructures. *Chemistry of Materials*, **18**, 4312–4318.

Ferrage, E. (2004) *Etude expérimentale de l'hydratation des smectites par simulation des raies 00l de diffraction des rayons X. Implications pour l'étude d'une perturbation thermique sur la minéralogie de l'argilite du site Meuse - Haute Marne*. PhD thesis, University of Grenoble, France, 326 pp.

Ferrage, E., Lanson, B., Malikova, N., Plançon, A., Sakharov, B.A. & Drits, V.A. (2005a) New insights on the distribution of interlayer water in bi-hydrated smectite from X-ray diffraction profile modeling of *00l* reflections. *Chemistry of Materials*, **17**, 3499–3512.

Ferrage, E., Lanson, B., Sakharov, B.A. & Drits, V.A. (2005b) Investigation of smectite hydration properties by modeling experimental X-ray diffraction patterns: Part I. Montmorillonite hydration properties. *American Mineralogist*, **90**, 1358–1374.

Ferrage, E., Tournassat, C., Rinnert, E., Charlet, L. & Lanson, B. (2005c) Experimental evidence for Ca-chloride ion pairs in the interlayer of montmorillonite. An XRD profile modeling approach. *Clays and Clay Minerals*, **53**, 348–360.

Ferrage, E., Tournassat, C., Rinnert, E. & Lanson, B. (2005d) Influence of pH on the interlayer cationic composition and hydration state of Ca-montmorillonite: Analytical chemistry, chemical modelling and XRD profile modelling study. *Geochimica et Cosmochimica Acta*, **69**, 2797–2812.

Ferrage, E., Kirk, C.A., Cressey, G. & Cuadros, J. (2007a) Dehydration of Ca-montmorillonite at the crystal scale. Part I: Structure evolution. *American Mineralogist*, **92**, 994–1006.

Ferrage, E., Kirk, C.A., Cressey, G. & Cuadros, J. (2007b) Dehydration of Ca-montmorillonite at the crystal scale. Part 2. Mechanisms and kinetics. *American Mineralogist*, **92**, 1007–1017.

Ferrage, E., Lanson, B., Sakharov, B.A., Geoffroy, N., Jacquot, E. & Drits, V.A. (2007c) Investigation of dioctahedral smectite hydration properties by modeling of X-ray diffraction profiles: Influence of layer charge and charge location. *American Mineralogist*, **92**, 1731–1743.

Ferrage, E., Lanson, B., Michot, L.J. & Robert, J.L. (2010) Hydration Properties and Interlayer Organization of Water and Ions in Synthetic Na-Smectite with Tetrahedral Layer Charge. Part 1. Results from X-ray Diffraction Profile Modeling. *Journal of Physical Chemistry C*, **114**, 4515–4526.

Ferrage, E., Sakharov, B.A., Michot, L.J., Delville, A., Bauer, A., Lanson, B., Grangeon, S., Frapper, G., Jimenez-Ruiz, M. & Cuello, G.J. (2011a) Hydration properties and interlayer organization of water and ions in synthetic Na-smectite with tetrahedral layer charge. Part 2. Towards a precise coupling between molecular simulations and diffraction data. *Journal of Physical Chemistry C*, **115**, 1867–1881.

Ferrage, E., Vidal, O., Mosser Ruck, R., Cathelineau, M. & Cuadros, J. (2011b) A reinvestigation of smectite illitization in experimental conditions: Results from X-ray diffraction and transmission electron microscopy. *American Mineralogist*, **96**, 207–223.

Fogg, A.M., Dunn, J.S. & O'Hare, D. (1998a) Formation of second-stage intermediates in anion-exchange intercalation reactions of the layered double hydroxide $[LiAl_2(OH)_6]Cl.H_2O$ as observed bu time-resolved, *in situ* X-ray diffraction. *Chemistry of Materials*, **10**, 356–360.

Fogg, A.M., Dunn, J.S., Shyu, S.-G., Cary, D.R. & O'Hare, D. (1998b) Selective ion-exchange intercalation of isomeric dicarboxylate anions into the layered double hydroxide $[LiAl_2(OH)_6]Cl.H_2O$. *Chemistry of Materials*, **10**, 351–355.

Gaillot, A.-C. (2002) *Caractérisation structurale de la birnessite: Influence du protocole de synthèse*. PhD thesis, University of Grenoble, France, 392 pp.

Gaillot, A.-C., Flot, D., Drits, V.A., Manceau, A., Burghammer, M. & Lanson, B. (2003) Structure of synthetic K-rich birnessite obtained by high-temperature decomposition of $KMnO_4$. I. Two-layer polytype from 800°C experiment. *Chemistry of Materials*, **15**, 4666–4678.

Gaillot, A.-C., Drits, V.A., Plançon, A. & Lanson, B. (2004) Structure of synthetic K-rich birnessites obtained by high-temperature decomposition of $KMnO_4$. 2. Phase and structural heterogeneities. *Chemistry of Materials*, **16**, 1890–1905.

Gaillot, A.-C., Lanson, B. & Drits, V.A. (2005) Structure of birnessite obtained from decomposition of permanganate under soft hydrothermal conditions. 1. Chemical and structural evolution as a function of temperature. *Chemistry of Materials*, **17**, 2959–2975.

Gaillot, A.-C., Drits, V.A., Manceau, A. & Lanson, B. (2007) Structure of the synthetic K-rich phyllomanganate birnessite obtained by high-temperature decomposition of KMnO4 - Substructures of K-rich birnessite from 1000°C experiment. *Microporous and Mesoporous Materials*, **98**, 267–282.

Gates, W.P., Slade, P.G., Manceau, A. & Lanson, B. (2002) Site occupancies by iron in nontronites. *Clays and Clay Minerals*, **50**, 223–239.

Glaeser, R., Mantine, I. & Méring, J. (1967) Observations sur la beidellite. *Bulletin du Groupe Français des Argiles*, **19**, 125–130.

Grangeon, S. (2008) *Cristallochimie des phyllomanganates nanocristallins désordonnés. Implication pour l'adsorption d'éléments métalliques*. PhD thesis, University of Grenoble, France, 210 pp.

Grangeon, S., Lanson, B., Lanson, M. & Manceau, A. (2008) Crystal structure of Ni-sorbed synthetic vernadite: a powder X-ray diffraction study. *Mineralogical Magazine*, **72**, 1279–1291.

Grangeon, S., Lanson, B., Miyata, N., Tani, Y. & Manceau, A. (2010) Structure of nanocrystalline phyllomanganates produced by freshwater fungi. *American Mineralogist*, **95**, 1608–1616.

Guerlou Demourgues, L., Tessier, C., Bernard, P. & Delmas, C. (2004) Influence of substituted zing on stacking faults in nickel hydroxide. *Journal of Materials Chemistry*, **14**, 2649–2654.

Guggenheim, S., Adams, J.M., Bain, D.C., Bergaya, F., Brigatti, M.F., Drits, V.A., Formoso, M.L.L., Galán, E., Kogure, T. & Stanjek, H. (2006) Summary of recommendations of nomenclature committees relevant to clay mineralogy: report of the Association Internationale pour l'Etude des Argiles (AIPEA) Nomenclature Committee for 2006. *Clay Minerals*, **41**, 863–877.

Guinier, A. (1964) *Théorie et technique de la radiocristallographie*. Dunod, Paris, 740 pp.

Hendricks, S. & Teller, E. (1942) X-ray interference in partially ordered layer lattices. *Journal of Chemical Physics*, **10**, 147–167.

Hower, J. & Mowatt, T.C. (1966) The mineralogy of illites and mixed-layer illite/montmorillonites. *American Mineralogist*, **51**, 825–854.

Hubert, F., Caner, L., Meunier, A. & Lanson, B. (2009) Advances in characterization of soil clay mineralogy using X-ray diffraction: from decomposition to profile fitting. *European Journal of Soil Science*, **60**, 1093–1105.

Hubert, F., Caner, L., Ferrage, E. & Meunier, A. (2011) Refinement of soil clay mineralogy based on the multispecimen XRD profile fitting procedure. *European Journal of Soil Science*, submitted.

Ijdo, W.L. & Pinnavaia, T.J. (1998a) Solid solution formation in amphiphilic organic-inorganic clay heterostructures. *Chemistry of Materials*, **11**, 3227–3231.

Ijdo, W.L. & Pinnavaia, T.J. (1998b) Staging of organic and inorganic gallery cations in layered silicate heterostructures. *Journal of Solid State Chemistry*, **139**, 281–289.

Ijdo, W.L., Lee, T. & Pinnavaia, T.J. (1996) Regularly interstratified layered silicate heterostructures: Precursors to pillared rectorite-like intercalates. *Advanced Materials*, **8**, 79–83.

Inoue, A., Bouchet, A., Velde, B. & Meunier, A. (1989) Convenient technique for estimating smectite layer percentage in randomly interstratified illite/smectite minerals. *Clays and Clay Minerals*, **37**, 227–234.

Inoue, A., Lanson, B., Marques Fernandes, M., Sakharov, B.A., Murakami, T., Meunier, A. & Beaufort, D. (2005) Illite-smectite mixed-layer minerals in the hydrothermal alteration of volcanic rocks: I. One-dimensional XRD structure analysis and characterization of component layers. *Clays and Clay Minerals*, **53**, 423–439.

Iwasaki, T. & Watanabe, T. (1988) Distribution of Ca and Na ions in dioctahedral smectites and interstratified dioctahedral mica/smectites. *Clays and Clay Minerals*, **36**, 73–82.

Iyi, N., Kurashima, K. & Fujita, T. (2002) Orientation of an organic anion and second-staging structure in layered double-hydroxide intercalates. *Chemistry of Materials*, **14**, 583–589.

Iyi, N., Fujii, K., Okatomo, K. & Sasaki, T. (2007) Factors influencing the hydration of layered double hydroxides (LDHs) and the appearance of an intermediate second staging phase. *Applied Clay Science*, **35**, 218–227.

Jagodzinski, H. (1949) Eindimensionale Fehlordnung in Kristallen und ihr Einfluss auf die Röntgeninterferenzen: I. Berechnung des Fehlordnungsgrades aus der Röntgenintensitaten. *Acta Crystallographica*, **2**, 201–207.

Jurgensen, A., Widmeyer, J.R., Gordon, R.A., Bendell Young, L.I., Moore, M.M. & Crozier, E.D. (2004) The structure of the manganese oxide on the sheath of the bacterium *Leptothrix discophora*: An XAFS study. *American Mineralogist*, **89**, 1110–1118.

Kakinoki, J. & Komura, Y. (1952) Intensity of X-ray diffraction by one dimensionally disordered crystal: I. General derivation in cases of the "Reichweit" $S = 0$ and 1. *Journal of the Physical Society of Japan*, **7**, 30–35.

Kakinoki, J. & Komura, Y. (1954a) Intensity of X-ray diffraction by one dimensionally disordered crystal: II. General derivation in the case of the correlation range $S \geq 2$. *Journal of the Physical Society of Japan*, **9**, 169–176.

Kakinoki, J. & Komura, Y. (1954b) Intensity of X-ray diffraction by one dimensionally disordered crystal: III. The close-packed structure. *Journal of the Physical Society of Japan*, **9**, 177–183.

Kakinoki, J. & Komura, Y. (1965) Diffraction by one dimensionally disordered crystal: I. The intensity equation. *Acta Crystallographica*, **19**, 137–147.

Kameda, J., Miyawaki, R., Kitagawa, R. & Kogure, T. (2007) XRD and HRTEM analyses of stacking structures in sudoite, di-trioctahedral chlorite. *American Mineralogist*, **92**, 1586–1592.

Kameda, J., Saruwatari, K., Beaufort, D. & Kogure, T. (2008) Textures and polytypes in vermiform kaolins diagenetically formed in a sandstone reservoir: a FIB-TEM investigation. *European Journal of Mineralogy*, **20**, 199–204.

Karmous, M.S., Ben Rhaiem, H., Robert, J.L., Lanson, B. & Amara, A.B.H. (2009) Charge location effect on the hydration properties of synthetic saponite and hectorite saturated by Na^{+}, Ca^{2+} cations: XRD investigation. *Applied Clay Science*, **46**, 43–50.

Kayenoshi, M. & Jones, W. (1998) Exchange of interlayer terephtalate anions from a Mg-Al layered double hydroxide: formation of intermediate intersratified phases. *Chemical Physics Letters*, **296**, 183–187.

Kogure, T. & Inoue, A. (2005) Determination of defect structures in kaolin minerals by high-resolution transmission electron microscopy (HRTEM). *American Mineralogist*, **90**, 85–89.

Kogure, T. & Kameda, J. (2008) High-resolution TEM and XRD simulation of stacking disorder in 2:1 phyllosilicates. *Zeitschrift für Kristallographie*, **223**, 69–75.

Kogure, T., Hybler, J. & Durovic, S. (2001) A HRTEM study of cronstedtite: Determination of polytypes and layer polarity in trioctahedral 1:1 phyllosilicates. *Clays and Clay Minerals*, **49**, 310–317.

Kogure, T., Jige, M., Kameda, J., Yamagishi, A., Miyawaki, R. & Kitagawa, R. (2006a) Stacking structures in pyrophyllite revealed by high-resolution transmission electron microscopy (HRTEM). *American Mineralogist*, **91**, 1293–1299.

Kogure, T., Kameda, J., Matsui, T. & Miyawaki, R. (2006b) Stacking structure in disordered talc: Interpretation of its X-ray diffraction pattern by using pattern simulation and high-resolution transmission electron microscopy. *American Mineralogist*, **91**, 1363–1370.

Kogure, T., Kameda, J. & Drits, V.A. (2008) Stacking faults with 180° layer rotation in celadonite, an Fe- and Mg-rich dioctahedral mica. *Clays and Clay Minerals*, **56**, 612–621.

Kogure, T., Elzea-Kogel, J., Johnston, C.T. & Bish, D.L. (2010) Stacking disorder in a sedimentary kaolinite. *Clays and Clay Minerals*, **58**, 62–71.

Lanson, B., Drits, V.A., Silvester, E.J. & Manceau, A. (2000) Structure of H-exchanged hexagonal birnessite and its mechanism of formation from Na-rich monoclinic buserite at low pH. *American Mineralogist*, **85**, 826–838.

Lanson, B., Drits, V.A., Feng, Q. & Manceau, A. (2002a) Structure of synthetic Na-birnessite: Evidence for a triclinic one-layer unit cell. *American Mineralogist*, **87**, 1662–1671.

Lanson, B., Drits, V.A., Gaillot, A.-C., Silvester, E., Plançon, A. & Manceau, A. (2002b) Structure of heavy-metal sorbed birnessite: Part 1. Results from X-ray diffraction. *American Mineralogist*, **87**, 1631–1645.

Lanson, B., Sakharov, B.A., Claret, F. & Drits, V.A. (2005) Diagenetic evolution of clay minerals in Gulf Coast shales: New insights from X-ray diffraction profile modeling. In: *Proceedings of the 42nd Annual Meeting, Clay Minerals Society (Burlington, Vermont, USA)*, p. 69.

Lanson, B., Marcus, M.A., Fakra, S., Panfili, F., Geoffroy, N. & Manceau, A. (2008) Formation of Zn-Ca phyllomanganate nanoparticles in grass roots. *Geochimica et Cosmochimica Acta*, **72**, 2478–2490.

Lanson, B., Sakharov, B.A., Claret, F. & Drits, V.A. (2009) Diagenetic smectite-to-illite transition in clay-rich sediments: a reappraisal of X-ray diffraction results using the multi-specimen method. *American Journal of Science*, **309**, 476–516.

Leoni, M. (2008) Diffraction analysis of layer disorder. *Zeitschift für Kristallographie*, **223**, 561–568.

Leoni, M., Gualtieri, A.F. & Roveri, N. (2004) Simultaneous refinement of structure and microstructure of layered materials. *Journal of Applied Crystallography*, **37**, 166–173.

Leroux, F. & Besse, J.-P. (2004) Layered double hydroxide/polymer nanocomposites. In: *Clay Surfaces: Fundamentals and Applications* (F. Wypych & K.G. Satyanarayana, editors). Elsevier, Amsterdam, pp. 459–495.

Lindgreen, H., Drits, V.A., Sakharov, B.A., Salyn, A.L., Wrang, P. & Dainyak, L.G. (2000) Illite-smectite structural changes during metamorphism in black Cambrian Alum shales from the Baltic area. *American Mineralogist*, **85**, 1223–1238.

Lindgreen, H., Drits, V.A., Sakharov, B.A., Jakobsen, H.J., Salyn, A.L., Dainyak, L.G. & Kroyer, H. (2002) The structure and diagenetic transformation of illite-smectite and chlorite-smectite from North Sea Cretaceous-Tertiary chalk. *Clay Minerals*, **37**, 429–450.

Lindgreen, H., Drits, V.A., Jakobsen, F.C. & Sakharov, B.A. (2008) Clay mineralogy of the Central North Sea Upper Cretaceous-Tertiary Chalk and the formation of clay-rich layers. *Clays and Clay Minerals*, **56**, 693–710.

Ma, C. & Eggleton, R.A. (1999) Surface layer types of kaolinite: A high-resolution transmission electron microscope study. *Clays and Clay Minerals*, **47**, 181–191.

MacEwan, D.M.C. (1956) Fourier transform methods for studying X-ray scattering from lamellar systems: I. A direct method for analysing interstratified mixtures. *Kolloidzeitschrift*, **149**, 96–108.

Makovicky, E. & Hyde, B.G. (1992) Incommensurate two-layer structures with complex crystal chemistry. *Materials Science Forum*, **100–101**, 1–100.

Manceau, A., Gorshkov, A.I. & Drits, V.A. (1992) Structural Chemistry of Mn, Fe, Co, and Ni in Mn hydrous oxides. II. Information from EXAFS spectroscopy, electron and X-ray diffraction. *American Mineralogist*, **77**, 1144–1157.

Manceau, A., Drits, V.A., Silvester, E.J., Bartoli, C. & Lanson, B. (1997) Structural mechanism of Co^{2+} oxidation by the phyllomanganate buserite. *American Mineralogist*, **82**, 1150–1175.

Manceau, A., Drits, V.A., Lanson, B., Chateigner, D., Wu, J., Huo, D., Gates, W.P. & Stucki, J.W. (2000a) Oxidation-reduction mechanism of iron in dioctahedral smectites: II. Crystal chemistry of reduced Garfield nontronite. *American Mineralogist*, **85**, 153–172.

Manceau, A., Lanson, B., Drits, V.A., Chateigner, D., Gates, W.P., Wu, J., Huo, D. & Stucki, J.W. (2000b) Oxidation-reduction mechanism of iron in dioctahedral smectites: I. Crystal chemistry of oxidized reference nontronites. *American Mineralogist*, **85**, 133–152.

McCarty, D.K. & Reynolds, R.C., Jr (1995) Rotationally disordered illite/smectite in Paleozoic K-bentonites. *Clays and Clay Minerals*, **43**, 271–284.

McCarty, D.K., Drits, V.A., Sakharov, B., Zviagina, B.B., Ruffell, A. & Wach, G. (2004) Heterogeneous mixed-layer clays from the Cretaceous greensand, Isle of Wight, southern England. *Clays and Clay Minerals*, **52**, 552–575.

McCarty, D.K., Sakharov, B.A. & Drits, V.A. (2008) Early clay diagenesis in Gulf Coast sediments: New insights from XRD profile modeling. *Clays and Clay Minerals*, **56**, 359–379.

McCarty, D.K., Sakharov, B.A. & Drits, V.A. (2009) New insights into smectite illitization: A zoned K-bentonite revisited. *American Mineralogist*, **94**, 1653–1671.

Méring, J. (1949) L'interférence des rayons-X dans les systèmes à stratification désordonnée. *Acta Crystallographica*, **2**, 371–377.

Méring, J. & Brindley, G.W. (1967) X-ray diffraction band profiles of montmorillonite. Influence of hydration and of the exchangeable cations. *Clays and Clay Minerals*, **15**, 51–60.

Méring, J. & Glaeser, R. (1954) Sur le rôle de la valence des cations échangeables dans la montomorillonite. *Bulletin de la Société Française de Minéralogie et de Cristallographie*, **77**, 519–530.

Meunier, A. (2006) Why are clay minerals small? *Clay Minerals*, **41**, 551–566.

Meunier, A., Lanson, B. & Velde, B. (2004) Composition variation of illite-vermiculite-smectite mixed-layer minerals in a bentonite bed from Charente (France). *Clay Minerals*, **39**, 317–332.

Möller, M.W., Handge, U.A., Kunz, D.A., Lunkenbein, T., Altstädt, V. & Breu, J. (2010a) Tailoring shear-stiff, mica-like nanoplatelets. *ACS Nano*, **4**, 717–724.

Möller, M.W., Hirsemann, D., Haarmann, F., Senker, J. & Breu, J. (2010b) Facile Scalable Synthesis of Rectorites. *Chemistry of Materials*, **22**, 186–196.

Moore, D.M. & Hower, J. (1986) Ordered interstratification of dehydrated and hydrated Na-smectite. *Clays and Clay Minerals*, **34**, 379–384.

Moore, D.M. & Reynolds, R.C., Jr (1997) *X-ray Diffraction and the Identification and Analysis of Clay Minerals*. Oxford University Press, New York, 378 pp.

Murakami, T., Inoue, A., Lanson, B., Meunier, A. & Beaufort, D. (2005) Illite-smectite mixed-layer minerals in the hydrothermal alteration of volcanic rocks: II. One-dimensional HRTEM structure images and formation mechanisms. *Clays and Clay Minerals*, **53**, 440–451.

Newman, S.P., Williams, S.J., Coveney, P.V. & Jones, W. (1998) Interlayer arrangement of hydrated MgAl layered double hydroxides containing guest terephtalate anions: Comparison of simulation and measurement. *Journal of Physical Chemistry B*, **102**, 6710–6719.

O'Hare, D., Evans, J.S.O., Fogg, A.M. & O'Brien, S. (2000) Time-resolved, *in situ* X-ray diffraction studies of intercalation in lamellar hosts. *Polyhedron*, **19**, 297–305.

Organova, N.I. (1989) *Crystal Chemistry of Incommensurate and Modulated Mixed-layer Minerals*. Nauka, Moscow, (in Russian), 140 pp.

Organova, N.I., Drits, V.A. & Dimitrik, A.L. (1974) Selected-area electron diffraction study of a type II "valleriite-like" mineral. *American Mineralogist*, **59**, 190–200.

Oueslati, W., Ben Rhaiem, H., Lanson, B. & Amara, A.B. (2009) Selectivity of Na-montmorillonite in relation with the concentration of bivalent cation (Cu^{2+}, Ca^{2+}, Ni^{2+}) by quantitative analysis of XRD patterns. *Applied Clay Science*, **43**, 224–227.

Perry, E.A., Jr. & Hower, J. (1970) Burial diagenesis in Gulf Coast pelitic sediments. *Clays and Clay Minerals*, **18**, 165–177.

Pevear, D.R. & Schuette, J.F. (1993) Inverting the Newmod X-ray diffraction forward model for clay minerals using genetic algorithms. In: *Computer Applications to X-ray Powder Diffraction Analysis of Clay Minerals* (R.C. Reynolds, Jr & J.R. Walker, editors). CMS workshop lectures, **5**. The Clay Minerals Society, Boulder, Colorado, USA.

Pisson, J., Taviot-Gueho, C., Israeli, Y., Leroux, F., Munsch, P., Itie, J.P., Briois, V., Morel-Desrosiers, N. & Besse, J.P. (2003) Staging of organic and inorganic anions in layered double hydroxides. *Journal of Physical Chemistry B*, **107**, 9243–9248.

Plançon, A. (1981) Diffraction by layer structures containing different kinds of layers and stacking faults. *Journal of Applied Crystallography*, **14**, 300–304.

Plançon, A. (2002) New modeling of X-ray diffraction by disordered lamellar structures, such as phyllosilicates. *American Mineralogist*, **87**, 1672–1677.

Plançon, A. (2003) Modelling X-ray diffraction by lamellar structures composed of electrically charged layers. *Journal of Applied Crystallography*, **36**, 146–153.

Plançon, A. & Drits, V.A. (1994) Expert system for structural characterization of phyllosilicates. I. Description of the expert system. *Clay Minerals*, **29,** 33–38.

Plançon, A. & Drits, V.A. (2000) Phase analysis of clays using an expert system and calculation programs for X-ray diffraction by two- and three-component mixed-layer minerals. *Clays and Clay Minerals*, **48**, 57–62.

Plançon, A. & Roux, J. (2010) Software for the assisted determination of the structural parameters of mixed-layer phyllosilicates. *European Journal of Mineralogy*, **22**, 733–740.

Plançon, A. & Tchoubar, C. (1977) Determination of structural defects in phyllosilicates by X-ray powder diffraction – II. Nature and proportion of defects in natural kaolinites. *Clays and Clay Minerals*, **25**, 436–450.

Plançon, A., Drits, V.A., Sakharov, B.A., Gilan, Z.I. & Ben Brahim, J. (1983) Powder diffraction by layered minerals containing different layers and/or stacking defects. Comparison between Markovian and non-Markovian models. *Journal of Applied Crystallography*, **16**, 62–69.

Plançon, A., Sakharov, B.A. & Drits, V.A. (1984a) Diffraction effects from a homogeneous aggregate of fine crystals with packing effects. *Soviet Physics Crystallography*, **29**, 392–395.

Plançon, A., Sakharov, B.A., Gilan, Z.I. & Drits, V.A. (1984b) Diffraction effects from a homogeneous aggregate of mixed-layer crystals. *Soviet Physics Crystallography*, **29**, 389–392.

Plançon, A., Giese, R.F., Snyder, R., Drits, V.A. & Bookin, A.S. (1989) Stacking faults in the kaolin-group minerals: Defect structures of kaolinite. *Clays and Clay Minerals*, **37**, 203–210.

Pons, C.H., Rousseaux, F. & Tchoubar, D. (1981) Utilisation du rayonnement synchrotron en diffusion aux petits angles pour l'étude du gonflement des smectites: I. Etude du système eau-montmorillonite-Na en fonction de la température. *Clay Minerals*, **16**, 23–42.

Pons, C.H., Rousseaux, F. & Tchoubar, D. (1982) Utilisation du rayonnement synchrotron en diffusion aux petits angles pour l'étude du gonflement des smectites: II. Etude de différents systèmes eau-smectites en fonction de la température. *Clay Minerals*, **17**, 327–338.

Radha, A.V. & Kamath, P.V. (2009) Polytype selection and structural disorder mediated by intercalated sulfate ions among the layered double hydroxides of Zn with Al and Cr. *Crystal Growth and Design*, **9**, 3197–3203.

Radha, A.V., Shivakumara, C. & Kamath, P.V. (2005) DIFFaX simulations of stacking faults in layered double hydroxides (LDHs). *Clays and Clay Minerals*, **53**, 520–527.

Radha, A.V., Antonyraj, C.A., Kamath, P.V. & Kannan, S. (2010) Polytype transformations in the SO_4^{2-} containing layered double hydroxides of Zinc with Aluminum and Chromium: The metal hydroxide layer as a structural synthon. *Zeitschrift Fur Anorganische Und Allgemeine Chemie*, **636**, 2658–2664.

Ragavan, A., Williams, G.R. & O'Hare, D. (2009) A thermodynamically stable layered double hydroxide heterostructure. *Journal of Materials Chemistry*, **19**, 4211–4216.

Rajamathi, M., Kamath, P.V. & Seshadri, R. (2000) Polymorphism in nickel hydroxide: role of interstratification. *Journal of Materials Chemistry*, **10**, 503–506.

Ramesh, T.N. (2009) Crystallite size effects in stacking faulted nickel hydroxide and its electrochemical behaviour. *Materials Chemistry and Physics*, **114**, 618–623.

Ramesh, T.N. & Kamath, P.V. (2008a) The effect of stacking faults on the electrochemical performance of nickel hydroxide electrodes. *Materials Research Bulletin*, **43**, 2827–2832.

Ramesh, T.N. & Kamath, P.V. (2008b) Planar defects in layered hydroxides: Simulation and structure refinement of beta-nickel hydroxide. *Materials Research Bulletin*, **43**, 3227–3233.

Ramesh, T.N., Jayashree, R.S. & Kamath, P.V. (2003) Disorder in layered hydroxides: DIFFaX simulation of the X-ray powder diffraction patterns of nickel hydroxide. *Clays and Clay Minerals*, **51**, 570–576.

Ramesh, T.N., Kamath, P.V. & Shivakumara, C. (2005) Correlation of structural disorder with the reversible discharge capacity of nickel hydroxide electrode. *Journal of the Electrochemical Society*, **152**, A806–A810.

Ramesh, T.N., Kamath, P.V. & Shivakumara, C. (2006) Classification of stacking faults and their stepwise elimination during the disorder ⇒ order transformation of nickel hydroxide. *Acta Crystallographica*, **B62**, 530–536.

Reynolds, R.C., Jr. (1967) Interstratified clay systems: Calculation of the total one-dimensional diffraction function. *American Mineralogist*, **52**, 661–672.

Reynolds, R.C., Jr. (1980) Interstratified clay minerals. In: *Crystal Structures of Clay Minerals and their X-ray Identification* (G.W. Brindley & G. Brown, editors). Monograph **5**, Mineralogical Society, London, pp. 249–359.

Reynolds, R.C., Jr. (1989) Diffraction by small and disordered crystals. In: *Modern Powder Diffraction* (D.L. Bish & J.E. Post, editors). Reviews in Mineralogy, **20**, Mineralogical Society of America, Washington, D.C., pp. 145–181.

Reynolds, R.C., Jr. (1993) Three-dimensional X-ray powder diffraction from disordered illite: Simulation and interpretation of the diffraction patterns. In: *Computer Applications to X-ray Powder Diffraction Analysis of Clay Minerals* (R.C. Reynolds, Jr & J.R. Walker, editors). Clay Minerals Society workshop lectures, **5**. The Clay Minerals Society, Boulder, Colorado, USA, pp. 44–78.

Rietveld, H.M. (1967) Line profiles of neutron-diffraction peaks for structure refinement. *Acta Crystallographica*, **22**, 151–152.

Rives, V. (2001) Layered double hydroxides: Present and future. Nova Science Publishers, New York, 439 pp.

Sakharov, B.A. (2005) Improved model for simulation of experimental XRD patterns for clays including mixed-layer clay minerals. In: *Proceedings of the Clay Minerals Society 42nd Annual Meeting (Burlington, Vermont, USA)*, p. 95.

Sakharov, B.A. & Drits, V.A. (1973) Mixed-layer kaolinite-montmorillonite: A comparison of observed and calculated diffraction patterns. *Clays and Clay Minerals*, **21**, 15–17.

Sakharov, B.A., Naumov, A.S. & Drits, V.A. (1982a) X-ray intensities scattered by layer structures with short-range ordering parameters $S \geq 1$ and $G \geq 1$. *Doklady Akademii Nauk*, **265**, 871–874 (in Russian).

Sakharov, B.A., Naumov, A.S. & Drits, V.A. (1982b) X-ray diffraction by mixed-layer structures with random distribution of stacking faults. *Doklady Akademii Nauk*, **265**, 339–343 (in Russian).

Sakharov, B.A., Lindgreen, H., Salyn, A. & Drits, V.A. (1999a) Determination of illite-smectite structures using multispecimen X-ray diffraction profile fitting. *Clays and Clay Minerals*, **47**, 555–566.

Sakharov, B.A., Lindgreen, H., Salyn, A.L. & Drits, V.A. (1999b) Mixed-layer kaolinite-illite-vermiculite in North Sea shales. *Clay Minerals*, **34**, 333–344.

Sakharov, B.A., Plançon, A. & Drits, V.A. (1999c) Influence of outer surface structure of crystals on X-ray diffraction. In: *Proceedings of the Euroclay conference (Krakow, Poland)*, p. 129.

Sakharov, B.A., Dubinska, E., Bylina, P., Kozubowski, J.A., Kapron, G. & Frontczak & Baniewicz, M. (2004a) Serpentine-smectite interstratified minerals from Lower Silesia (SW Poland). *Clays and Clay Minerals*, **52**, 55–65.

Sakharov, B.A., Plançon, A., Lanson, B. & Drits, V.A. (2004b) Influence of the outer surface layers of crystals on the X-ray diffraction intensity of basal reflections. *Clays and Clay Minerals*, **52**, 680–692.

Sato, T., Watanabe, T. & Otsuka, R. (1992) Effects of layer charge, charge location, and energy change on expansion properties of dioctahedral smectites. *Clays and Clay Minerals*, **40**, 103–113.

Sato, T., Murakami, T. & Watanabe, T. (1996) Change in layer charge of smectites and smectite layers in illite/smectite during diagenetic alteration. *Clays and Clay Minerals*, **44**, 460–469.

Scherrer, P. (1918) Bestimmung der Grösse und der inneren Struktur von Kolloidteilchen mittels Röntgenstrahlen. *Nachrichten von der Gesellschaft der Wissenschaften zu Göttingen, Mathematisch-Physikalische Kl.*, 98–100 (in German).

Skipper, N.T., Chang, F.R.C. & Sposito, G. (1995) Monte Carlo simulation of interlayer molecular structure in swelling clay minerals. 1. Methodology. *Clays and Clay Minerals*, **43**, 285–293.

Slade, P.G., Stone, P.A. & Radoslovitch, E.W. (1985) Interlayer structures of the two-layer hydrates of Na- and Ca-vermiculites. *Clays and Clay Minerals*, **33**, 51–61.

Smith, D.E. (1998) Molecular computer simulations of the swelling properties and interlayer structure of cesium montmorillonite. *Langmuir*, **14**, 5959–5967.

Środoń, J. (1980) Precise identification of illite/smectite interstratifications by X-ray powder diffraction. *Clays and Clay Minerals*, **28**, 401–411.

Środoń, J. (1984) X-ray powder diffraction of illitic materials. *Clays and Clay Minerals*, **32**, 337–349.

Sudo, T. & Shimoda, S. (1977) Interstratified clay minerals – Mode of occurrence and origin. *Minerals Science Engineering*, **9**, 3–24.

Taviot-Guého, C., Leroux, F., Payen, C. & Besse, J.-P. (2005) Cationic ordering and second-staging in copper-chromium and zinc-chromium layered double hydroxides. *Applied Clay Science*, **28**, 111–120.

Taviot-Guého, C., Feng, Y., Faour, A. & Leroux, F. (2010) Intercalation chemistry in a LDH system: anion exchange process and staging phenomenon investigated by means of time-resolved, *in situ* X-ray diffraction. *Dalton Transactions*, **39**, 5994–6005.

Tessier, C., Haumesser, P.H., Bernard, P. & Delmas, C. (1999) The structure of $Ni(OH)_2$: From the ideal material to the electrochemically active one. *Journal of the Electrochemical Society*, **146**, 2059–2067.

Tessier, C., Guerlou Demourgues, L., Faure, C., Basterreix, M., Nabias, G. & Delmas, C. (2000a) Structural and textural evolution of zinc-substituted nickel hydroxide electrode materials upon ageing in KOH and upon redox cycling. *Solid State Ionics*, **133**, 11–23.

Tessier, C., Guerlou Demourgues, L., Faure, C., Demourgues, A. & Delmas, C. (2000b) Structural study of zinc-substituted nickel hydroxides. *Journal of Materials Chemistry*, **10**, 1185–1193.

Thomas, G.S., Rajamathi, M. & Kamath, P.V. (2004) DIFFaX simulations of polytypism and disorder in hydrotalcite. *Clays and Clay Minerals*, **52**, 693–699.

Thomas, G.S. & Kamath, P.V. (2006) Line broadening in the PXRD patterns of layered hydroxides: The relative effects of crystallite size and structural disorder. *Journal of Chemical Sciences*, **118**, 127–133.

Treacy, M.M.J., Newsam, J.M. & Deem, M.W. (1991) A general recursion method for calculating diffracted intensities from crystals containing planar faults. *Proceedings of the Royal Society of London*, **433**, 499–520.

Tsipursky, S.J. & Drits, V.A. (1984) The distribution of octahedral cations in the 2:1 layers of dioctahedral smectites studied by oblique-texture electron diffraction. *Clay Minerals*, **19**, 177–193.

Tsipursky, S.J., Eberl, D.D. & Buseck, P.R. (1992) Unusual tops (bottoms?) of particles of 1M illite from the Silverton caldera (CO). In: *Proceedings of the American Society of Agronomy Annual Meeting*. American Society of Agronomy, Madison, Wisconsin, USA, pp. 381–382.

Tsybulya, S.V., Cherepanova, S.V. & Kryukova, G.N. (2004) Full profile analysis of X-ray diffraction patterns for investigation of nanocrystalline systems. In: *Diffraction Analysis of the Microstructure of Materials* (E.J. Mittemeijer & P. Scardi, editors). Springer Verlag, Berlin, pp. 93–123.

Ufer, K., Roth, G., Kleeberg, R., Stanjek, H., Dohrmann, R. & Bergmann, J. (2004) Description of X-ray powder pattern of turbostratically disordered layer structures with a Rietveld compatible approach. *Zeitschift für Kristallographie*, **219**, 519–527.

Ufer, K., Kleeberg, R., Bergmann, J., Curtius, H. & Dohrmann, R. (2008) Refining real structure parameters of disordered layer structures within the Rietveld method. *Zeitschift für Kristallographie*, **S27**, 151–158.

Ufer, K., Kleeberg, R., Bergmann, J. & Dohrmann, R. (2010) Simultaneous refinement of multi-device and/or multi-specimen XRD data of mixed layered structures. In: *Proceedings of the SEA-CSSJ-CMS trilateral meeting on clays (Sevilla)*, p. 46.

Ulibarri, M.A. & Hermosín, M.C. (2001) Layered double hydroxides in water decontamination. In: *Layered Double Hydroxides: Present and Future* (V. Rives, editor). Nova Science Publishers, New York, pp. 251–284.

Vaccari, A. (1998) Preparation and catalytic properties of cationic and anionic clays. *Catalysis Today*, **41**, 53–71.

Velde, B., Suzuki, T. & Nicot, E. (1986) Pressure-temperature-composition of illite/smectite mixed-layer minerals: Niger delta mudstones and other examples. *Clays and Clay Minerals*, **34**, 435–441.

Viani, A., Gaultieri, A.F. & Artioli, G. (2002) The nature of disorder in montmorillonite by simulation of X-ray powder patterns. *American Mineralogist*, **87**, 966–975.

Villalobos, M., Lanson, B., Manceau, A., Toner, B. & Sposito, G. (2006) Structural model for the biogenic Mn oxide produced by *Pseudomonas putida. American Mineralogist*, **91**, 489–502.

Walker, G.F. (1956) The mechanism of dehydration of Mg-vermiculite. *Clays and Clay Minerals*, **5**, 101–115.

Warren, B.E. (1941) X-ray diffraction in random layer lattices. *Physical Review*, **59**, 693–698.

Watanabe, T. (1981) Identification of illite/montmorillonite interstratification by X-ray powder diffraction. *Journal of the Mineralogical Society of Japan*, **15**, 32–41.

Watanabe, T. (1988) The structural model of illite/smectite interstratified mineral and the diagram for their identification. *Clay Science*, **7**, 97–114.

Webb, S.M., Tebo, B.M. & Bargar, J.R. (2005) Structural characterization of biogenic Mn oxides produced in seawater by the marine *Bacillus sp*. strain SG-1. *American Mineralogist*, **90**, 1342–1357.

Williams, G.R. & O'Hare, D. (2005) Factors influencing staging during anion-exchange intercalation into $[LiAl_2(OH)_6]X \bullet mH_2O$ ($X = Cl^-$, Br^-, NO_3^-). *Chemistry of Materials*, **17**, 2632–2640.

Williams, G.R. & O'Hare, D. (2006) Towards understanding, control and application of leyered double hydroxide chemistry. *Journal of Materials Chemistry*, **16**, 3065–3074.

Williams, G.R., Norquist, A.J. & O'Hare, D. (2003) The formation of ordered heterostructues during the intercalation of phosphonic acids into a double layered hydroxide. *Chemical Communications*, 1816–1817.

Williams, G.R., Norquist, A.J. & O'Hare, D. (2004) Time-resolved, in situ X-ray diffraction studies of staging during phosphonic acid intercalation into $[LiAl_2(OH)_6]Cl \cdot H_2O$. *Chemistry of Materials*, **16**, 975–981.

Zhang, W., He, J. & Guo, C. (2008) Second staging of tartrate and carbonate anions in Mg–Al layered double hydroxide. *Applied Clay Science*, **39**, 166–171.

Zhu, M., Ginder-Vogel, M., Feng, X.H. & Sparks, D.L. (2010) Cation effects on the layer structure of biogenic Mn-oxides. *Environmental Science & Technology*, **44**, 4465–4471.